JCB Journal of Cell Biology

ARTICLE

Branched actin networks push against each other at adherens junctions to maintain cell–cell adhesion

Nadia Efimova and Tatyana M. Svitkina

Adherens junctions (AJs) are mechanosensitive cadherin-based intercellular adhesions that interact with the actin cytoskeleton and carry most of the mechanical load at cell–cell junctions. Both Arp2/3 complex–dependent actin polymerization generating pushing force and nonmuscle myosin II (NMII)-dependent contraction producing pulling force are necessary for AJ morphogenesis. Which actin system directly interacts with AJs is unknown. Using platinum replica electron microscopy of endothelial cells, we show that vascular endothelial (VE)-cadherin colocalizes with Arp2/3 complex–positive actin networks at different AJ types and is positioned at the interface between two oppositely oriented branched networks from adjacent cells. In contrast, actin–NMII bundles are located more distally from the VE-cadherin–rich zone. After Arp2/3 complex inhibition, linear AJs split, leaving gaps between cells with detergent-insoluble VE-cadherin transiently associated with the gap edges. After NMII inhibition, VE-cadherin is lost from gap edges. We propose that the actin cytoskeleton at AJs acts as a dynamic push–pull system, wherein pushing forces maintain extracellular VE-cadherin transinteraction and pulling forces stabilize intracellular adhesion complexes.

Introduction

Compartmentalization of tissues in an organism is mediated by cohesive monolayers of epithelial and endothelial cells. Both cell types create a barrier at the tissue boundary, but an endothelial barrier is more dynamic and permits solute exchange and leukocyte transmigration (Giannotta et al., 2013; Schnittler et al., 2014). Inadequate control of endothelial permeability leads to edema that accompanies inflammation, allergy, ischemia, and other disorders (Dejana and Giampietro, 2012).

Cells control monolayer permeability by forming various cell–cell adhesions. Among them, adherens junctions (AJs) carry most of the mechanical load (Huveneers and de Rooij, 2013; Twiss and de Rooij, 2013; Ladoux et al., 2015). AJs are formed by adhesion receptors, mainly of the cadherin family, and strengthened by the actin cytoskeleton, which interacts with cadherins through α- and β-catenins and other components of the cadherin adhesion complex (Twiss and de Rooij, 2013; Padmanabhan et al., 2015; Mège and Ishiyama, 2017). To build AJs, epithelial and vascular-endothelial cells use epithelial cadherin (E-cadherin) and vascular endothelial (VE)-cadherin, respectively. AJs are often classified into punctate (discontinuous) and linear (continuous) AJs that are typical for remodeling and cohesive cell sheets, respectively (Twiss and de Rooij, 2013). Because of more active junction remodeling, endothelial AJs exhibit greater polymorphism than epithelial cells, with a greater fraction of punctate AJs.

Actin cytoskeleton is important for stabilization, remodeling, and mechanosensitive properties of AJs (Michael and Yap, 2013; Schnittler et al., 2014; Hoffman and Yap, 2015; Ladoux et al., 2015; Röper, 2015). As the major force-generating machinery in the cell, the actin cytoskeleton can produce both pulling and pushing forces (Svitkina, 2018). Pulling (contractile) forces in nonmuscle cells are generated by sliding of bipolar filaments of nonmuscle myosin II (NMII) along actin filaments. Generation of pushing (protrusive) forces most commonly involves polymerization of actin filaments organized into branched networks by the Arp2/3 complex (Pollard, 2007; Svitkina, 2013).

The NMII-generated contractile force applied to AJ is required for their stabilization (Twiss and de Rooij, 2013; Ladoux et al., 2015). The best understood mechanosensor at AJs is α-catenin, which can unfold under force (Yonemura et al., 2010; Barry et al., 2014; Buckley et al., 2014; Yao et al., 2014), allowing for recruitment of additional adhesion complex components (Yonemura et al., 2010; Twiss et al., 2012; Thomas et al., 2013; Yao et al., 2014; Oldenburg et al., 2015), long-range clustering of cadherin (Chen et al., 2015), and stabilization and elaboration of AJs (Liu et al., 2010). The presence of contractile actin bundles at AJs is well established. In epithelial cells, mature linear AJs are typically flanked by tangential (parallel to the AJ) actin–NMII bundles located immediately next to the junctional plasma membranes

Department of Biology, University of Pennsylvania, Philadelphia, PA.

Correspondence to Tatyana Svitkina: svitkina@sas.upenn.edu.

(Hull and Staehelin, 1979; Hirokawa and Tilney, 1982; Yonemura, 2011). In assembling AJs, tangential bundles can be located at a distance from the cadherin-rich zone and connected to the AJs by small oblique bundles approaching the AJ at various angles (Yonemura et al., 1995). The latter organization is often exhibited by linear AJs of endothelial cells, although more mature configurations resembling linear AJs of epithelial cells are also present (Huveneers et al., 2012). Punctate AJs in both cell types are associated with oblique actin–NMII bundles (often referred to as "radial") that form end-on attachments with the cadherin-rich foci (Millán et al., 2010; Huveneers et al., 2012).

The roles of Arp2/3 complex–dependent actin polymerization in AJ morphogenesis are mostly discussed in relation to AJ remodeling. Lamellipodia driven by polymerizing branched actin networks allow cells to come into physical contact (Krendel and Bonder, 1999; Ehrlich et al., 2002; Ayollo et al., 2009; Hoelzle and Svitkina, 2012), expand the area of cell–cell interaction (Ehrlich et al., 2002; Yamada and Nelson, 2007), and heal the intercellular gaps (Martinelli et al., 2013; Abu Taha et al., 2014). In assembling AJs, a faint population of dynamic F-actin is located at the cadherin-rich zone between tangential actin bundles (Yonemura et al., 1995; Adams et al., 1998; Krendel and Bonder, 1999; Zhang et al., 2005) and contains proteins typical for Arp2/3 complex–dependent protrusions (Kovacs et al., 2002; Helwani et al., 2004; Verma et al., 2004; Yamazaki et al., 2007). In mature AJs, however, actin polymerization is thought to become obsolete (Mège et al., 2006; Ryu et al., 2009) because both protrusive activity of cells and the signaling pathways that activate actin polymerization are down-regulated upon AJ maturation (Ehrlich et al., 2002; Yamada and Nelson, 2007; Ayollo et al., 2009). Nonetheless, functional experiments indicate that Arp2/3 complex–dependent polymerization machinery is required for maintenance of mature AJs (Sahai and Marshall, 2002; Ivanov et al., 2005; Furman et al., 2007; Gates et al., 2007; Yamazaki et al., 2007; Kovacs et al., 2011; Tang and Brieher, 2012; Lee et al., 2016).

Specific roles of Arp2/3 complex–dependent machinery at AJs are not clear. Conceptually, if only contractile forces acted at mature AJs, the AJs would be unstable and prone to separation. Indeed, both excessive activation and inhibition of cell contractility impairs mature AJs, although punctate AJs can be strengthened as a result of mechanostimulation (Krendel et al., 1999; Sahai and Marshall, 2002; Shewan et al., 2005; Ayollo et al., 2009; Huveneers et al., 2012; Naydenov et al., 2016). It is typically assumed that contractile forces at AJs can be counterbalanced just by cadherin-mediated adhesion (Twiss and de Rooij, 2013; Schnittler et al., 2014), but protrusive forces were also proposed as a possibility (Yap et al., 2015). However, direct evidence for the existence of such protrusive forces at mature AJs is lacking as is a conceptual understanding of the interplay between pushing and pulling at AJs.

One way to understand the relative roles of pulling and pushing forces at AJs is to determine spatial distribution of actin cytoskeleton components responsible for protrusion and contraction. EM is a powerful approach to attain this goal. Besides being able to precisely localize molecular markers by immunolabeling, EM has a potential to distinguish structural features of protrusive and contractile actin arrays. Protrusive actin networks formed by Arp2/3 complex consist of short branched filaments with a ∼70° angle between their barbed ends oriented in the direction of protrusion (Svitkina et al., 1997; Svitkina and Borisy, 1999). Conversely, contractile actin structures consist of long unbranched actin filaments that often form tight bundles (Svitkina et al., 1995; Verkhovsky et al., 1995). Traditional thin-section EM can visualize actin bundles reasonably well, especially large and stable ones (Sanger and Sanger, 1980; Tilney et al., 1980). However, visualization of branched actin networks by conventional EM techniques is challenging because of the fragility of these networks and their complex 3D architecture. Among various EM approaches, platinum replica EM (PREM), which combines the high resolution of EM with an ability to preserve three-dimensionality (Svitkina, 2017), has been most productive in revealing branched actin filament networks at various subcellular locations and in different cells (Svitkina and Borisy, 1999; Cameron et al., 2001; Korobova and Svitkina, 2010; Collins et al., 2011; Svitkina, 2017).

In this study, we used PREM in combination with immunogold labeling to determine actin cytoskeleton organization at cell–cell junctions of human umbilical vein endothelial cells (HUVECs). We show that Arp2/3 complex–positive branched actin networks represent the actin cytoskeleton component that is commonly associated with VE-cadherin at both linear and punctate AJs. In contrast, NMII-containing actin bundles are typically linked to the VE-cadherin–rich zone through branched networks. In mature linear AJs, a thin junctional strip of branched networks consists of two oppositely oriented network populations originating from two adjacent cells, whereas VE-cadherin is enriched at the interface between these colliding networks. The structure and dynamics of cell–cell junctions after inhibition of Arp2/3 complex activity or NMII-dependent contractility suggest that branched networks at AJs push against each other to promote VE-cadherin transinteraction, whereas contractile activity of NMII stabilizes cadherin complexes at the AJ cytoplasmic face.

Results

General organization of the actin cytoskeleton at different types of AJs

HUVECs form both linear and punctate AJs (Huveneers et al., 2012). We stained HUVECs with phalloidin and antibodies to VE-cadherin and vasodilator-stimulated phosphoprotein (VASP) to characterize their AJs by fluorescence microscopy. VASP is an actin elongation factor that in cells localizes to sites of actin polymerization (Dominguez, 2009). In migrating cells, VASP is highly enriched in focal adhesions at the ends of contractile stress fibers (Reinhard et al., 1992). A lower level of VASP is present at the leading edge of lamellipodia (Rottner et al., 1999). This difference in VASP enrichment in the bundled and branched actin arrays can help to roughly discriminate these actin subsets based on the level of VASP immunofluorescence.

VE-cadherin staining in HUVECs revealed both linear and punctate AJs (Fig. 1). As expected, punctate AJs were associated with oblique actin bundles (Fig. 1, C and F), whereas linear AJs were often flanked by tangential actin bundles (Fig. 1, B and E), usually located at some distance from the VE-cadherin–positive

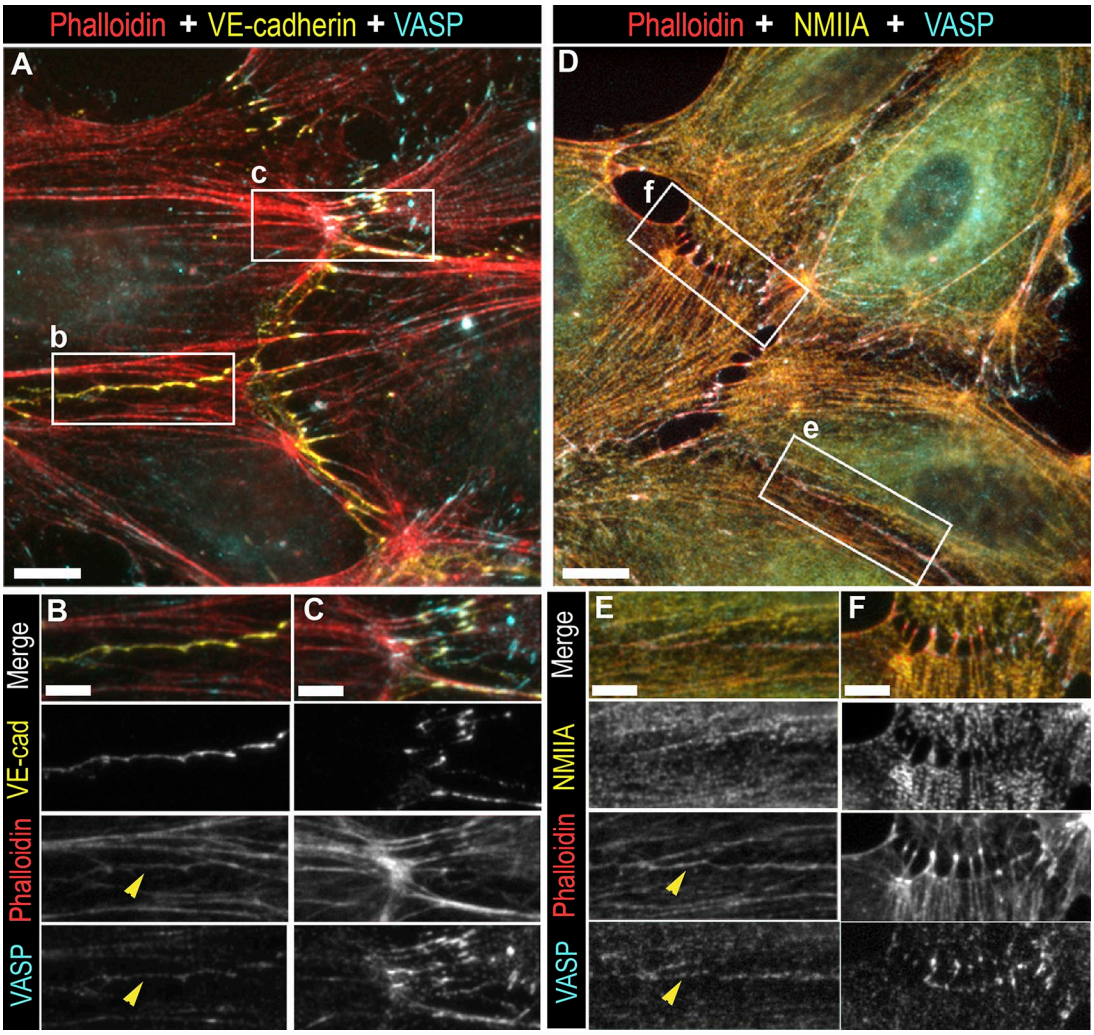

Figure 1. **Fluorescence microscopy of actin cytoskeleton components at AJs in HUVECs. (A–C)** Costaining with phalloidin (red) and antibodies to VE-cadherin (yellow) and VASP (cyan). **(D–F)** Costaining with phalloidin (red) and antibodies to NMIIA (yellow) and VASP (cyan). Boxed regions in A and D outline linear (b and e) and punctate (c and f) AJs and are enlarged in B, C, E, and F, respectively. Arrowheads in B and E mark linear AJs. Bars: (A and D) 10 µm; (B, C, E, and F) 5 µm.

line. Additionally, a faint F-actin signal colocalized with the linear VE-cadherin–rich zone (Fig. 1, B and E). VASP colocalized with VE-cadherin at both punctate and linear AJs, but exhibited bright staining at punctate AJs (Fig. 1 C), suggesting their association with bundled actin filaments, and faint labeling at linear AJs (Fig. 1 B), suggesting the presence of branched actin networks there.

To examine the contractile actin cytoskeleton at AJs, we costained HUVECs with phalloidin and an antibody to NMIIA, the most abundant isoform of NMII (Fig. 1 D). NMIIA staining was hardly detectable in linear AJs marked by faint continuous staining of VASP and F-actin (Fig. 1 E) but was prominently present in both tangential and oblique actin bundles (Fig. 1, E and F).

To test whether linear VE-cadherin distributions in HUVECs correspond with mature or assembling AJs, we performed live-cell imaging of GFP–VE-cadherin and mCherry-LifeAct (an F-actin marker) in HUVECs. We found that linear GFP–VE-cadherin patterns located between adjacent or more distally positioned tangential bundles overlap with a faint dynamic strip of mCherry-LifeAct fluorescence and exhibit subtle dynamics. However, they do not undergo gross changes over time periods up to 60 min, suggesting that such AJs are fully formed and stable (Videos 1, 2, and 6).

Linear AJs coincide with a strip of branched actin network flanked by actin–NMII bundles

We next analyzed cytoskeleton structure at cell–cell junctions by PREM. Because contractile actin bundles are thought to be most intimately associated with AJs, we combined PREM with immunogold staining of NMIIA. We first focused on linear AJs, which were identified morphologically at low EM magnification (Fig. 2 A). A conventional signature of mature AJs in epithelial cells is the presence of tangential actin–NMII bundles closely flanking a continuous linear distribution of cadherin. Such conventional linear AJs are less common, but still present, in endothelial cells.

High-magnification views of linear AJs exhibiting a classic appearance showed three sets of actin structures: two bundles

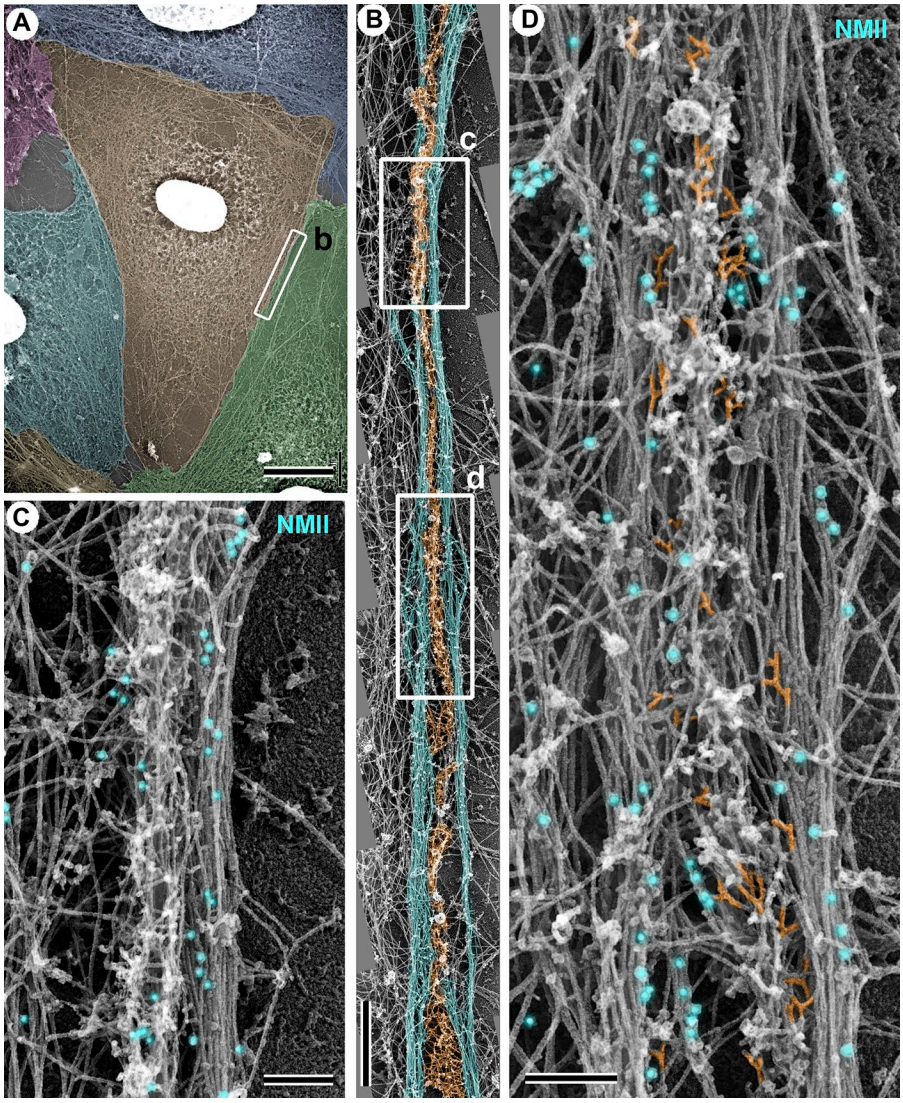

Figure 2. **PREM of linear AJs. (A)** Overview of a cell (shaded in brown) that forms linear AJs with three neighboring cells (green, blue, and cyan) and also contacts the fourth cell (red). The boxed region is enlarged in B. **(B)** Linear AJ contains a narrow strip of branched network (orange) flanked by two actin-NMII bundles (cyan). Boxed regions are enlarged in C and D, respectively. **(C and D)** NMIIA immunogold (18 nm, cyan) and some actin branches (D, orange) are pseudocolored. Bars: (A) 10 µm; (B) 1 µm; (C and D) 200 nm.

of long actin filaments labeled intermittently with NMIIA immunogold and a narrow strip of unlabeled actin network between these bundles (Fig. 2, B–D). The presence of Y-shaped actin filament branches, short filaments, and abundant filament ends in this network (Fig. 2, C and D) suggested an Arp2/3 complex–dependent actin array. Based on analysis of five linear AJs with a total length of 55 µm, the spacing between two flanking bundles could be as narrow as 100–300 nm. Sometimes, the bundles even appeared to touch each other, but even in such cases, a strip of branched actin network was present between the bundles (Fig. 2 C).

Not all linear junctions in HUVECs had this classic appearance, in which a branched actin strip was closely flanked by two parallel tangential bundles. In many cases, the tangential bundles were several micrometers apart and less perfectly aligned. Nonetheless, a narrow strip of branched actin network was consistently present between peripheral tangential bundles (Fig. S1). The connection between the tangential bundles and the strip of the branched network was mediated by oblique actin bundles or individual actin filaments, which merged with the branched strip at a variety of angles (Fig. S1, B and C).

These data show that a narrow strip of branched network is always present at continuous cell–cell contacts, which, based on morphological criteria, correspond with linear AJs.

VE-cadherin and α-catenin colocalize with the junctional strip of branched network

The PREM technique involves detergent extraction of cells, which exposes the cytoskeleton but dissolves the plasma membrane, thus making imprecise the morphological identification of cell–cell boundaries. To determine the exact location of the AJ, we performed double-immunogold staining of HUVECs with antibodies to VE-cadherin (18 nm gold; actual diameter is 15.8 ± 1.0 nm; mean ± SD; n = 100) and NMIIA (12 nm gold; actual diameter is 10.1 ± 0.6 nm; n = 100). These gold sizes can be unambiguously distinguished from each other and from upright actin filament ends that also appear as bright dots in inverse contrast, but unlike gold particles, they have a dark core (Fig. S2 A). Strikingly, VE-cadherin immunogold at linear AJs colocalized predominantly with the branched actin network (80.4 ± 6.4%; n = 2,393 gold particles in 15 segments of linear AJs with a total length of 152.4 µm from two experiments). In

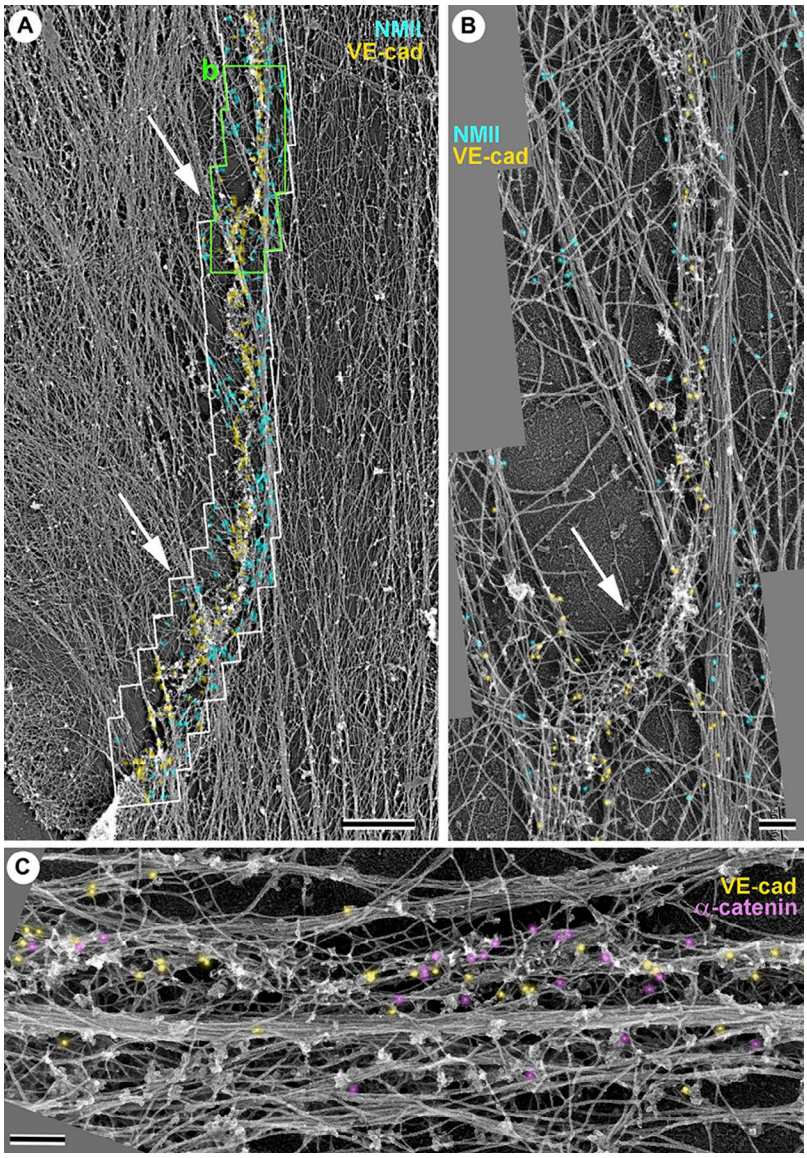

Figure 3. **Localization of VE-cadherin and α-catenin at linear AJs. (A)** Linear AJ labeled with VE-cadherin (18 nm, yellow) and NMIIA (12 nm, cyan) immunogold. The region outlined in white was analyzed at high magnification to locate gold particles. The region outlined in green is enlarged in B. **(B)** VE-cadherin immunogold (yellow) colocalizes predominantly with the branched strip even as the strip shifts from one bundle to another (arrow). Ends of oblique actin bundles near the branched strip are also occasionally labeled with VE-cadherin immunogold (arrows in A). NMIIA immunogold (cyan) labels tangential and oblique actin bundles. **(C)** VE-cadherin (18 nm, yellow) and α-catenin (12 nm, magenta) immunogold colocalize with each other on the branched actin network. Bars: (A) 2 µm; (B and C) 200 nm.

contrast, NMIIA immunogold labeled tangential and oblique actin bundles and barely overlapped with the VE-cadherin–positive regions (Fig. 3). Even when a strip of the branched network shifted away from one tangential actin bundle to another, VE-cadherin immunogold was still associated with the branched network, whereas tangential actin bundles exhibited negligible VE-cadherin labeling (Fig. 3 B). We did not encounter examples in which a linear stretch of VE-cadherin immunogold would reside on tangential bundles without branched actin networks present in the vicinity. The remaining (19.6 ± 6.4%) VE-cadherin gold particles, which were not associated with branched networks, were typically found along the distal parts of oblique actin bundles near their junction with the AJs (Fig. 3, A and B). These additional VE-cadherin gold particles produced local enrichments of VE-cadherin labeling along the length of the linear AJ, which likely reflected force-dependent local augmentation of the VE-cadherin adhesion complex (Liu et al., 2010). Interestingly, the strips of branched networks that were densely labeled with VE-cadherin immunogold were usually quite narrow (230 ± 108 nm wide; 14 linear AJs from three independent experiments with total length of 163 µm measured every ∼1 µm). In contrast, when cell–cell contacts were made by broad overlapping lamellipodia, VE-cadherin labeling was sparse (Fig. S2, B–D), suggesting that AJs in such cases were not fully formed. Despite its narrowness, the branched actin strip at AJs was as dense as branched actin network in lamellipodia at the free edges of HUVECs, although lamellipodia were much wider (0.5–2 µm wide). Quantification of the actin density (see Materials and methods) showed indistinguishable ($P = 0.08$) occupancy of the network area by actin filaments in both cases (lamellipodia: 67.5 ± 2.3%; six regions with total area of 13.1 μm^2; junctional strips: 64.5 ± 3.3%; seven regions with total area of 25.2 μm^2). These similar densities suggest that branched networks at AJs can be as efficient in exerting pushing force as those assembled in lamellipodia (Cojoc et al., 2007) and in reconstituted systems (Bieling et al., 2016).

Because VE-cadherin is linked to actin filaments indirectly, we examined localization of α-catenin, an actin-binding

component of the VE-cadherin adhesion complex. By both fluorescence microscopy (Fig. S3 A) and PREM (Figs. 3 C and S3 B), VE-cadherin and α-catenin at linear AJs colocalized with each other predominantly on branched networks.

For PREM experiments, we mostly analyzed AJs formed by cohesive cells in the middle of cell colonies in subconfluent HUVEC cultures. Such cells are better spread and exhibit fewer cell overlaps than cells in dense confluent cultures, which makes PREM of subconfluent cultures more interpretable. Nonetheless, in linear AJs formed in dense confluent HUVEC monolayers, VE-cadherin immunogold also localized to branched actin networks, and not to the adjacent actin bundles (Fig. S4). At other cell–cell boundaries in confluent cultures, VE-cadherin immunogold had broad distributions caused by significant overlapping of adjacent cells and assembly of adhesion complexes in the x–y plane between cells.

Junctional actin strip contains Arp2/3 complex and consists of two oppositely oriented branched networks

Although the presence of Y-shaped branches with an ∼70° angle between actin filaments (Fig. 2) is a reliable reporter of Arp2/3 complex–dependent actin polymerization in the junctional actin strip, we further validated this interpretation by double-immunogold staining of the Arpc2 subunit of the Arp2/3 complex (12-nm gold) and VE-cadherin (18-nm gold; Fig. 4). Both markers localized predominantly to the morphologically recognizable branched actin network and were scarce in adjacent cell regions (Fig. 4, B–D). A small fraction of VE-cadherin immunogold found outside the junctional strip (Fig. 4 D) was usually associated with ends of oblique actin bundles (Fig. 4 C). A small fraction of non-junctional Arpc2 immunogold (Fig. 4 D) corresponded with non-junctional branched network.

The orientation of actin branches shows direction of pushing force generated by branched networks. Close examination of the actin strip at linear AJs revealed two sets of branches oriented roughly against each other (Figs. 5 and S5). VE-cadherin immunogold tended to localize to the region of overlap between these two subsets (Fig. 5, C and D; and Fig. S5 C), indicating that they belonged to different contacting cells. Quantification of branch orientation showed that 55.8 ± 13.0% of branches were oriented toward the VE-cadherin–rich zone, 19.6 ± 10.1% were oriented away and 18.2 ± 11.0% were oriented parallel to the AJ (n = 1,222 branches in 15 segments of linear AJs with a total length of 35.7 µm from two independent experiments). Very rarely, we could observe a segment of the linear AJ, where a branched network from one cell collided with a tangential bundle of the neighboring cell and VE-cadherin localized approximately at the interface between the branched network and the bundle (Fig. S5 D). Typically, even when low-magnification images gave an impression that a lamellipodium of one cell is pushing against a bundle of the other cell (Fig. 5 B), high-magnification images showed that the "attacked" cell "defended" itself by sending a smaller lamellipodium with oppositely oriented actin filament branches to meet the attacker and that VE-cadherin was localized approximately to the area of collision (Fig. 5 D).

Punctate AJs contain branched actin networks as a component of their cytoskeleton

Punctate AJs are a diverse group. Their common feature is discontinuous VE-cadherin (Figs. 1 and 6) and α-catenin (Fig. S3, A and C–E) distribution and association with oblique actin-NMII bundles. Using the existing nomenclature with slightly modified definitions, we categorized punctate AJs into three groups: focal AJs, intercellular bridges, and engulfed fingers. Focal AJs have been previously defined as VE-cadherin clusters attached to radial ("oblique" in our terminology) actin–NMII bundles (Huveneers et al., 2012). We limit this category to cases in which cells still maintain an extended cell–cell contact without obvious gaps, even if VE-cadherin is discontinuous. If VE-cadherin clusters are flanked by intercellular gaps, we define them as intercellular bridges (Hoelzle and Svitkina, 2012). Engulfed fingers were described previously as VE-cadherin–rich linear extensions of one cell that appeared to be partially internalized by the neighboring cell (Hayer et al., 2016).

Focal AJs were associated with actin bundles terminating in the VE-cadherin–rich regions (Fig. 6 A). However, branched actin filaments of opposite orientation were also typically detected at the junction. These branched networks were often contiguous with the lamellipodia formed along the edge of each cell between focal AJs, but VE-cadherin labeling was low in these interstitial regions.

In intercellular bridges, VE-cadherin immunogold (Figs. 6 B and S6) could form a compact cluster (Fig. S6), but more commonly it was distributed along the associated actin bundles (Fig. 6 B). This distribution probably corresponded with a junction along the lateral surfaces of filopodium-like protrusions from neighboring cells (Hoelzle and Svitkina, 2012). Again, branched actin filaments often could be seen in the area labeled by VE-cadherin (Figs. 6 B and S6) as also confirmed by Arpc2 immunogold staining (Fig. 6 B).

Engulfed fingers (Fig. 6 C) appeared as a thin bundle of actin filaments extending from one cell underneath the neighboring cell. These extensions were labeled by VE-cadherin immunogold (Fig. 6 C). The edge of the engulfing cell formed a funnel-shaped lamellipodium that extended over the surface of the adjacent cell. In addition to labeling the finger-like extension, a significant amount of VE-cadherin immunogold was also present along the sides of the "funnel," apparently, where the engulfing cell encountered the base of the engulfed finger. Branched actin filaments were not readily apparent along the length of the engulfed finger. The funnel-shaped lamellipodium, however, contained abundant branched actin filaments oriented toward the neighboring cell. Branched actin filaments oriented in the opposite direction could be detected in the engulfed cell (Fig. 6 C).

Reticular AJs are associated with branched actin networks and small actin bundles

Endothelial cells often exhibit so-called reticular AJs (Cain et al., 2010; Seebach et al., 2015) with a polygonal distribution of VE-cadherin, which likely correspond with regions where neighboring cells overlap and present the lateral view of an AJ. Such

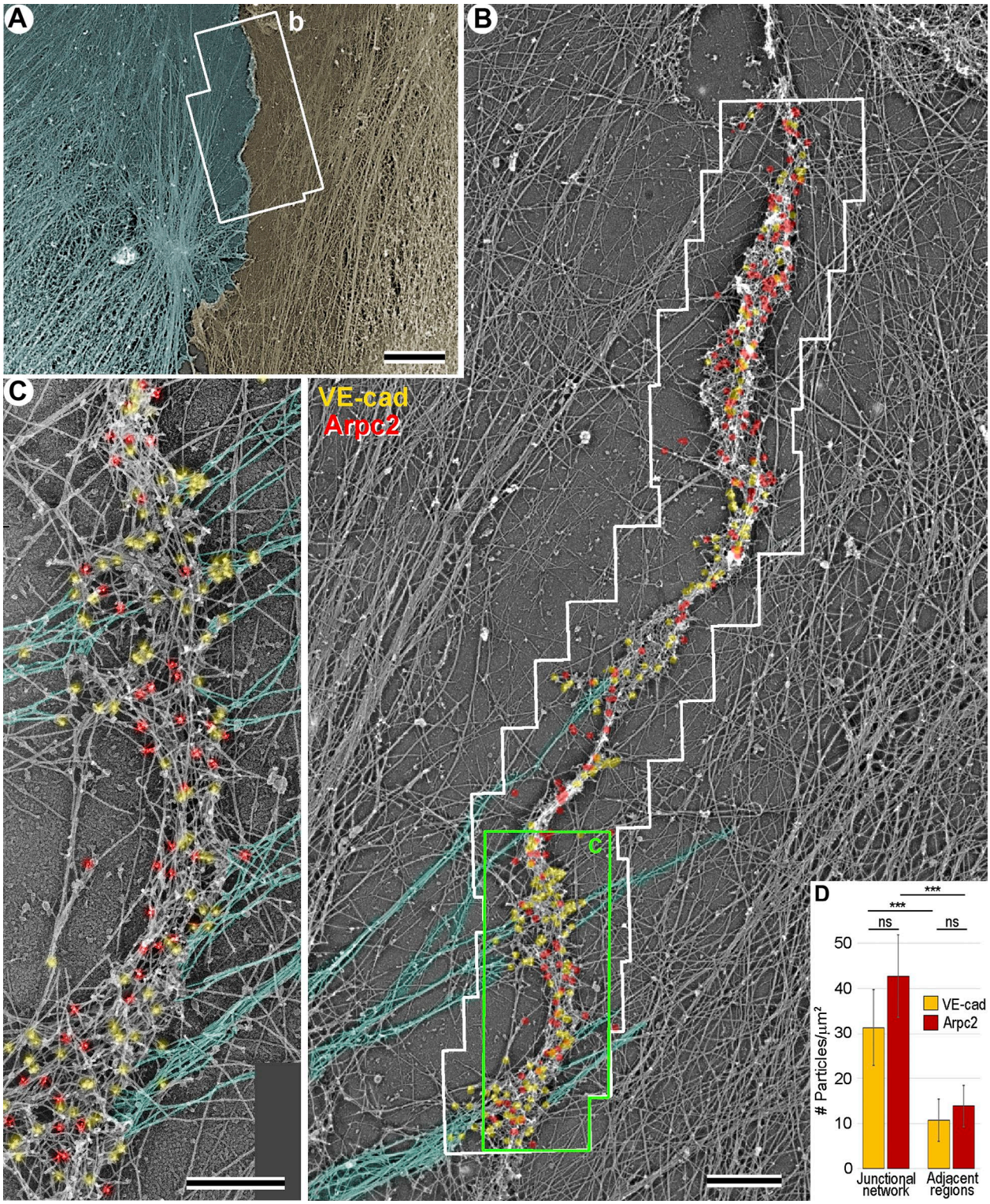

Figure 4. **Branched network at linear AJs contains Arp2/3 complex. (A)** Overview of a linear AJ between two pseudocolored cells. The outlined region is enlarged in B. **(B and C)** Distributions of Arpc2 (12 nm, red) and VE-cadherin (18 nm, yellow) immunogold largely colocalize with the junctional strip of branched actin network. The region outlined in white in B was analyzed at high magnification. Broad tangential bundles are located at a distance from the branched strip. Some oblique actin bundles and filaments joining the branched strip are highlighted in cyan. Region outlined in green is enlarged in C. Bars: (A) 5 µm; (B) 1 µm; (C) 500 nm. **(D)** Densities of VE-cadherin and Arpc2 immunogold per area occupied by the cytoskeleton within junctional networks and in adjacent cell regions. Error bars indicate SD; ***, $P < 0.001$. $n = 7$ PREM montages with total area of 90 µm² (25.2 µm² of junctional networks with 64.5 ± 3.3% [mean ± SD] coverage by the cytoskeleton and 64.4 µm² of adjacent regions with 33.8 ± 9.0% coverage by the cytoskeleton). Data distribution was normal by Kolmogorov–Smirnov normality test. Significance was determined by parametric Tukey–Kramer multiple comparisons test.

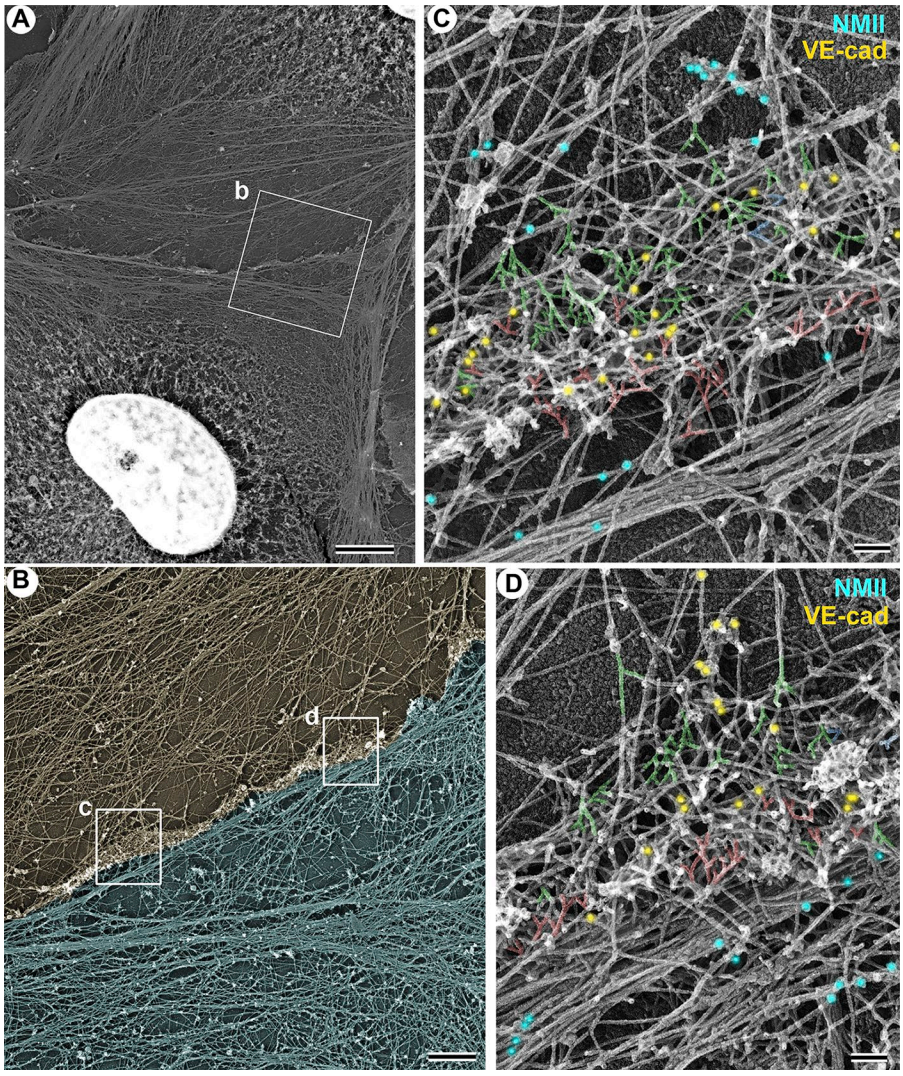

Figure 5. **Orientation of actin branches at linear AJs. (A)** Overview of a linear AJ between two cells. The boxed region is enlarged in B. **(B)** Lamellipodia from the attacking cell (shaded in yellow) collides with the tangential bundle of the defending cell (blue). Boxed regions are enlarged in C and D, respectively. **(C and D)** Double-immunogold labeling of NMIIA (12 nm, cyan) and VE-cadherin (18 nm, yellow). Actin branches at linear AJs contain two oppositely oriented sets. VE-cadherin immunogold is mostly located between these sets. Representative branches presumably originating from the blue and yellow cells are shaded in red and green, respectively; branches with neutral orientation are shaded in blue. Bars: (A) 5 µm; (B) 1 µm; (C and D) 100 nm.

AJs are particularly abundant in dense confluent HUVEC monolayers. By fluorescence microscopy, VE-cadherin at reticular AJs formed a network-like pattern, whereas phalloidin staining did not show any conspicuous distribution (Fig. S7 A). By PREM (Fig. S7, B–D), VE-cadherin distributions that appeared to correspond with reticular AJs colocalized with a loose network of actin filaments, which consisted of a complex arrangement of thin bundles, individual long actin filaments and Arpc2 immunogold labeled branched filaments (Fig. S7, C and D).

Arp2/3 complex activity is important for maintenance of linear AJs

Localization of VE-cadherin between colliding branched actin networks at linear AJs suggested that two cells might use Arp2/3 complex–dependent actin polymerization to push against each other in order to maintain contact. To test this idea, we treated HUVECs with the Arp2/3 complex inhibitor CK666. Fluorescence staining with phalloidin and cortactin antibody, a marker of branched actin networks, showed much weaker, but still detectable, staining of cortactin after treatment with 100 µM CK666 compared with control cells (Fig. S8 A). The presence of remaining lamellipodia in CK666-treated cells also indicated a partial inhibition of the Arp2/3 complex in these conditions. Immunofluorescence staining with VE-cadherin antibody (Fig. 7, A and B) revealed formation of multiple gaps between CK666-treated cells, with bright VE-cadherin puncta marking remaining cell–cell contacts (Fig. 7 B). Faint VE-cadherin signals apparently localizing to gap edges could sometimes be seen between these puncta (Fig. 7 B).

Live-cell imaging of HUVECs expressing GFP–VE-cadherin and mCherry-LifeAct showed that addition of CK666 caused cell–cell separation, which occurred either abruptly (44 of 65 cell–cell boundaries) or gradually (21 of 65 cell–cell boundaries), probably depending on intrinsic differences in cell contractility and/or adhesion in individual cells. Addition of DMSO as control did not affect cell–cell junctions (Video 2). Abrupt cell–cell separation was accompanied by overall cell retraction, with the formation and subsequent breakage of long intercellular bridges (Video 3). Gradual separation often began with thinning of the GFP–VE-cadherin–rich linear zone and was followed by slow formation of narrow intercellular gaps crossed by intermittent short VE-cadherin–rich bridges; a fainter VE-cadherin signal also transiently remained at the gap edges (Fig. 7, C and D; and Videos 4 and 5).

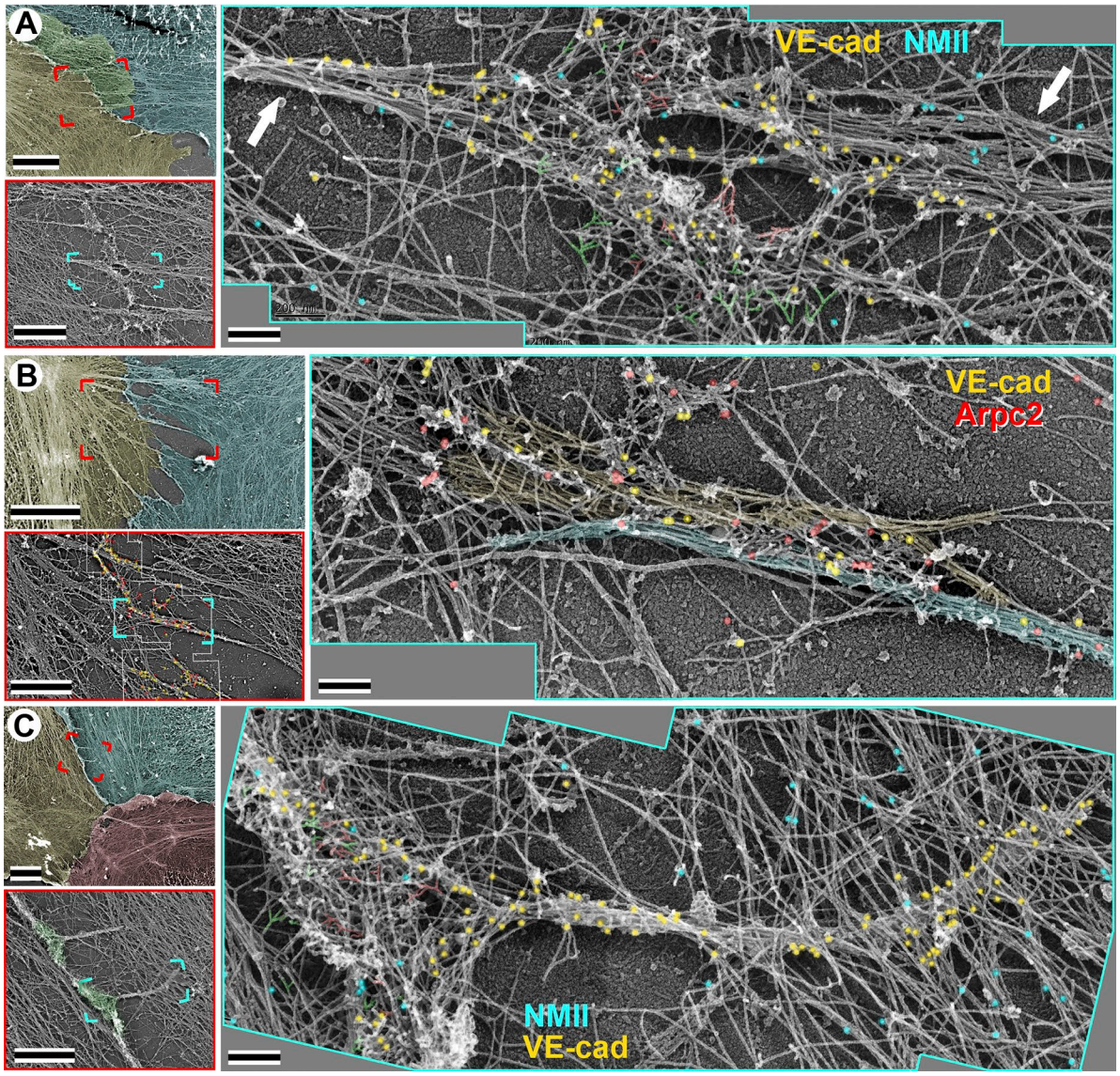

Figure 6. **Different types of punctate AJs contain branched actin networks. (A)** In focal AJs, VE-cadherin localizes at the tips of oblique actin bundles (arrows), where branched filaments are also present. **(B)** In intercellular bridges, Arp2/3 complex colocalizes with VE-cadherin along the lateral interface between two filopodium-like protrusions from adjacent cells shaded in yellow and blue, respectively. **(C)** In engulfed fingers, VE-cadherin is enriched along the linear extension of the yellow (engulfed) cell and within a funnel-shaped lamellipodium of the blue (engulfing) cell. Oppositely oriented actin branches (red and green) are present where the funnel-shaped lamellipodium overlaps with the base of the engulfed finger. Top left: Overviews of the junction area with pseudocolored individual cells. Cell overlap in A and funnel-shaped lamellipodia in C are shaded in green. Red-bracketed areas are enlarged in bottom left panels. Cyan-bracketed areas are enlarged in right panels. Double-immunogold staining of VE-cadherin (18 nm, yellow) and either NMIIA (A and C; 12 nm, cyan) or Arpc2 (B; 12 nm, red). Representative actin branches apparently coming from different cells are shaded in red and green, respectively (A and C). Bars: (top left) 5 µm; (bottom left) 2 µm; (right) 200 nm.

PREM also showed incomplete inhibition of branched actin nucleation by CK666. Prominent lamellipodia were still present at free cell edges, but they contained a sparser actin network. We focused on cell–cell interfaces that still preserved some interaction and appeared to correspond with the slow cell–cell separation mode induced by CK666 treatment (Fig. 8). In these cases, boundaries of adjacent cells ran almost parallel to each other at 0.3–2.5-µm distances (1.1 ± 0.6 µm; n = 10 intercellular gaps with a total length of 111 µm measured every 1–2 µm; Fig. 8, B and C), which could make a subset of these gaps undetectable by light microscopy. The gaps were sometimes crossed by VE-cadherin–positive bridges (Fig. 8, F and G). Consistent with a significant decrease of branched actin networks in CK666-treated cells, VE-cadherin immunogold was more prominently associated with actin bundles or loose unbranched actin filaments (75.7 ± 7.8%; n = 2,282 gold particles in 11 segments of adjacent cell–cell boundaries with total length of 118.7 µm) compared with control cells (19.6 ± 6.4%; see above). The rest of the gold particles (24.3 ± 7.8%) were associated with remaining branched networks. Besides labeling intercellular bridges, VE-cadherin could be often seen at the gap edges (Fig. 8, B–E). The unusual preservation of VE-cadherin at free cell edges after

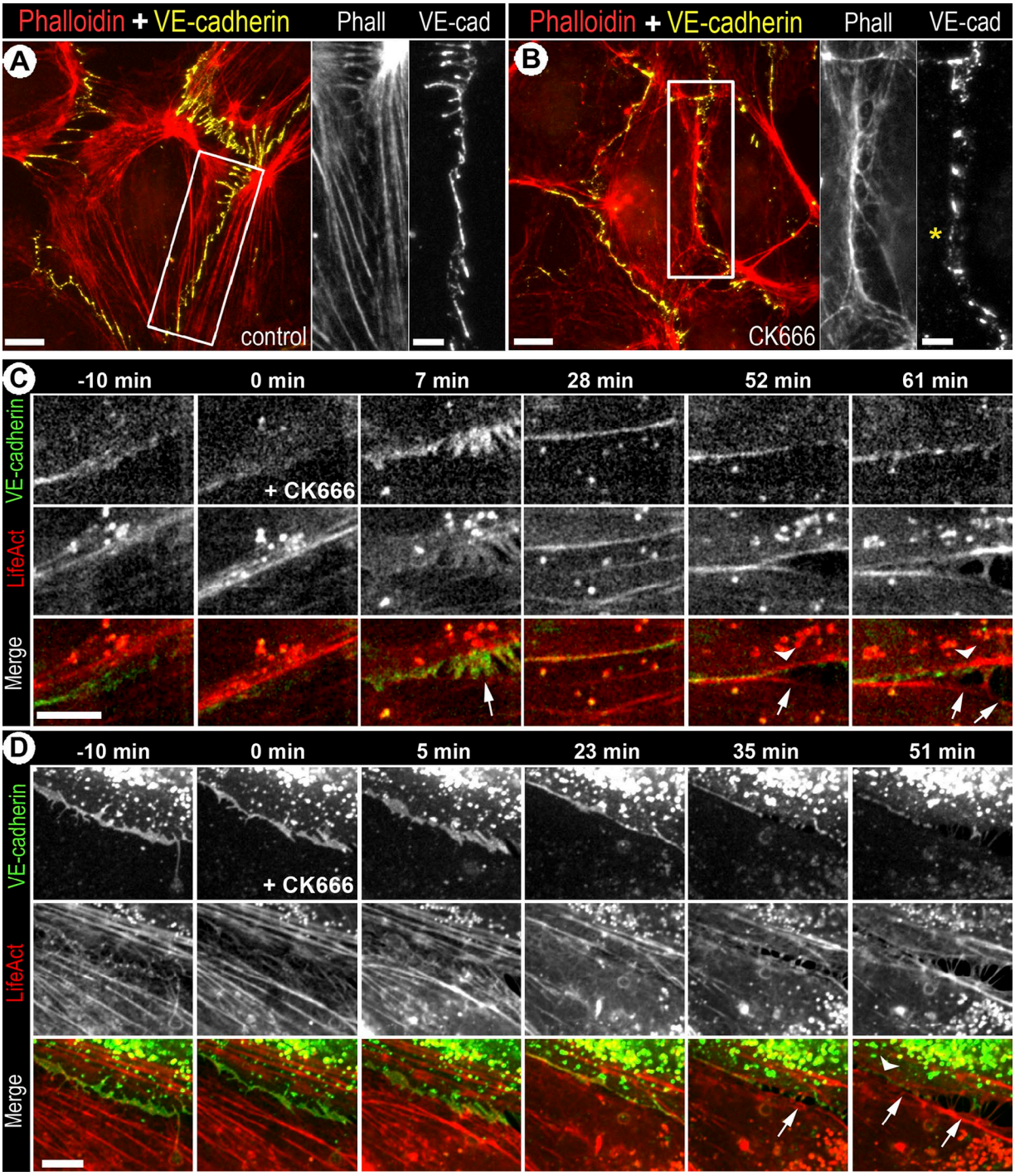

Figure 7. **Inhibition of the Arp2/3 complex leads to separation of linear AJs. (A and B)** Fluorescence staining of control HUVECs (A) and HUVECs treated with 100 µM CK666 (B) with phalloidin (red) and VE-cadherin antibody (yellow). Boxed regions in A and B are enlarged at right. The asterisk marks VE-cadherin at the edge of a gap. **(C and D)** Two examples of GFP–VE-cadherin (green) and mCherry-LifeAct (red) dynamics at AJs in the course of CK666 treatment. CK666 was added at time 0. Arrows mark CK666-induced intercellular gaps; arrowheads mark VE-cadherin at gap edges. Bars: (A and B, left, and C and D) 10 µm; (A and B, right) 5 µm.

detergent extraction suggests that VE-cadherin–catenin complexes are still connected to the cytoskeleton despite the loss of adhesion. Indeed, in some cases, it was possible to observe a non-filamentous material associated with VE-cadherin immunogold at gap edges (Fig. 8, D and E), which could correspond with VE-cadherin–catenin complexes.

Because of incomplete inhibition of the Arp2/3 complex in our conditions, we labeled CK666-treated cells with cortactin immunogold to evaluate the degree of local inhibition of branched nucleation. In control HUVECs, cortactin immunogold, as expected, labeled the junctional strip of the branched actin network (Fig. S8, B–D). In CK666-treated cells, cortactin

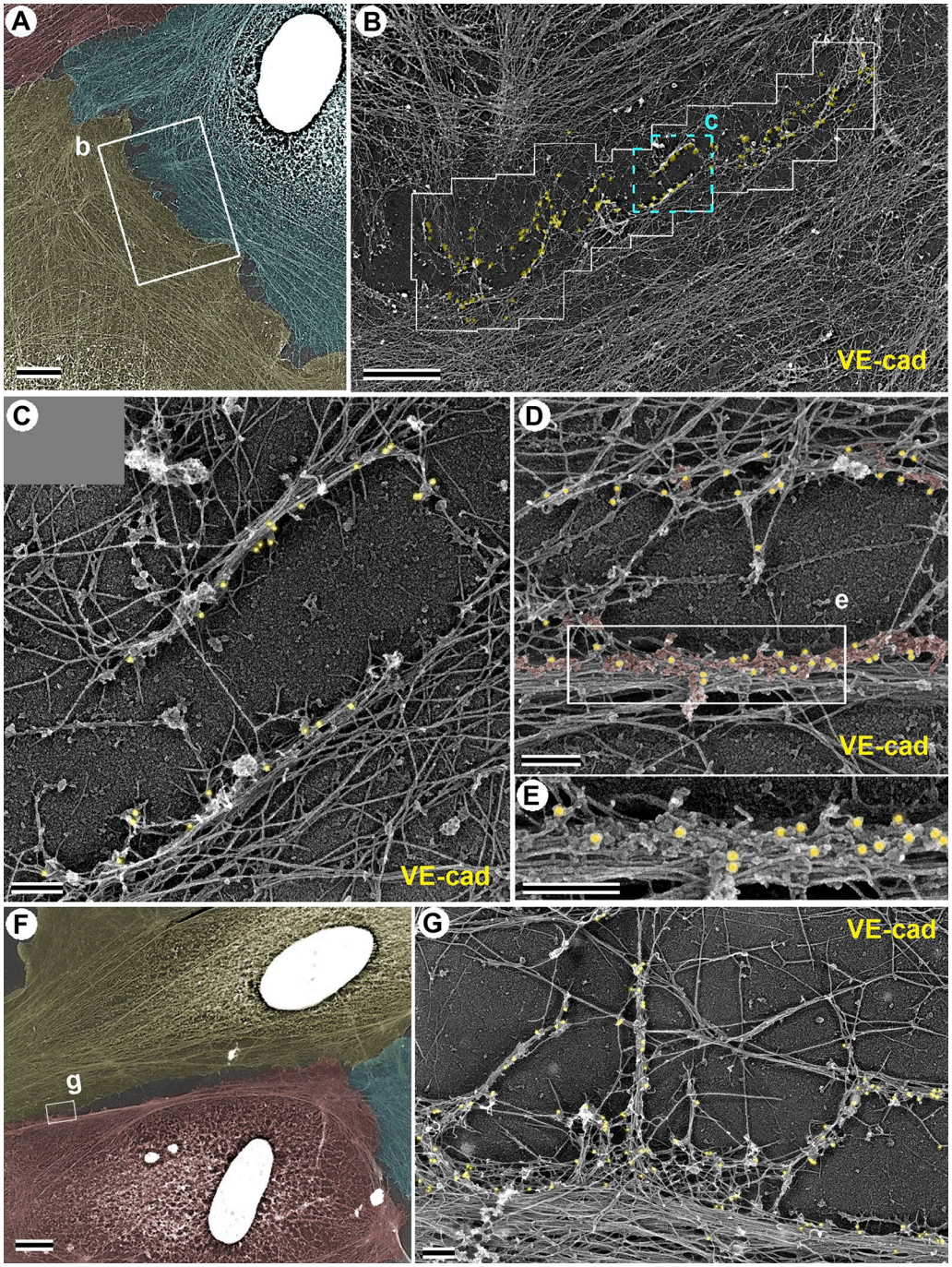

Figure 8. **PREM of VE-cadherin distribution after CK666 treatment. (A and F)** Overviews of the cell–cell interfaces with pseudocolored individual cells. Gaps between cells remain gray. Outlined regions are enlarged in B and G, respectively. **(B)** VE-cadherin immunogold (18 nm, yellow) labels both sides of the intercellular gap. The region outlined in white was analyzed at high magnification to locate gold particles. The region outlined in cyan is enlarged in C. **(C and G)** VE-cadherin is associated with the gap edges (C) and intercellular bridges (G). **(D and E)** VE-cadherin immunogold at gap edges associates with non-filamentous material (shaded red in D) residing on the actin bundle. The boxed region in D is enlarged in E. Bars: (A and F) 5 µm; (B) 2 µm; (C–E and G) 200 nm.

localized to the remaining cell–cell junctions, whereas free gap edges were less efficiently labeled (Fig. S8, E–G). These data suggest a correlation between down-regulation of branched networks and loss of cell–cell adhesion. Overall, the effects of CK666 suggest that after Arp2/3 complex inhibition, linear AJs split along the cell–cell interface as if resulting from impaired VE-cadherin transinteraction in the intercellular space, whereas cytoplasmic VE-cadherin–containing adhesion complexes transiently remain associated with the cytoskeleton despite cell–cell separation.

Inhibition of cell contractility impairs AJs and leads to a loss of VE-cadherin from edges of intercellular gaps

To determine how cell contractility affects cytoskeletal architecture of AJs, we treated HUVECs with the NMII inhibitor blebbistatin (Fig. 9, A and B) or the Rho-associated protein kinase (ROCK)

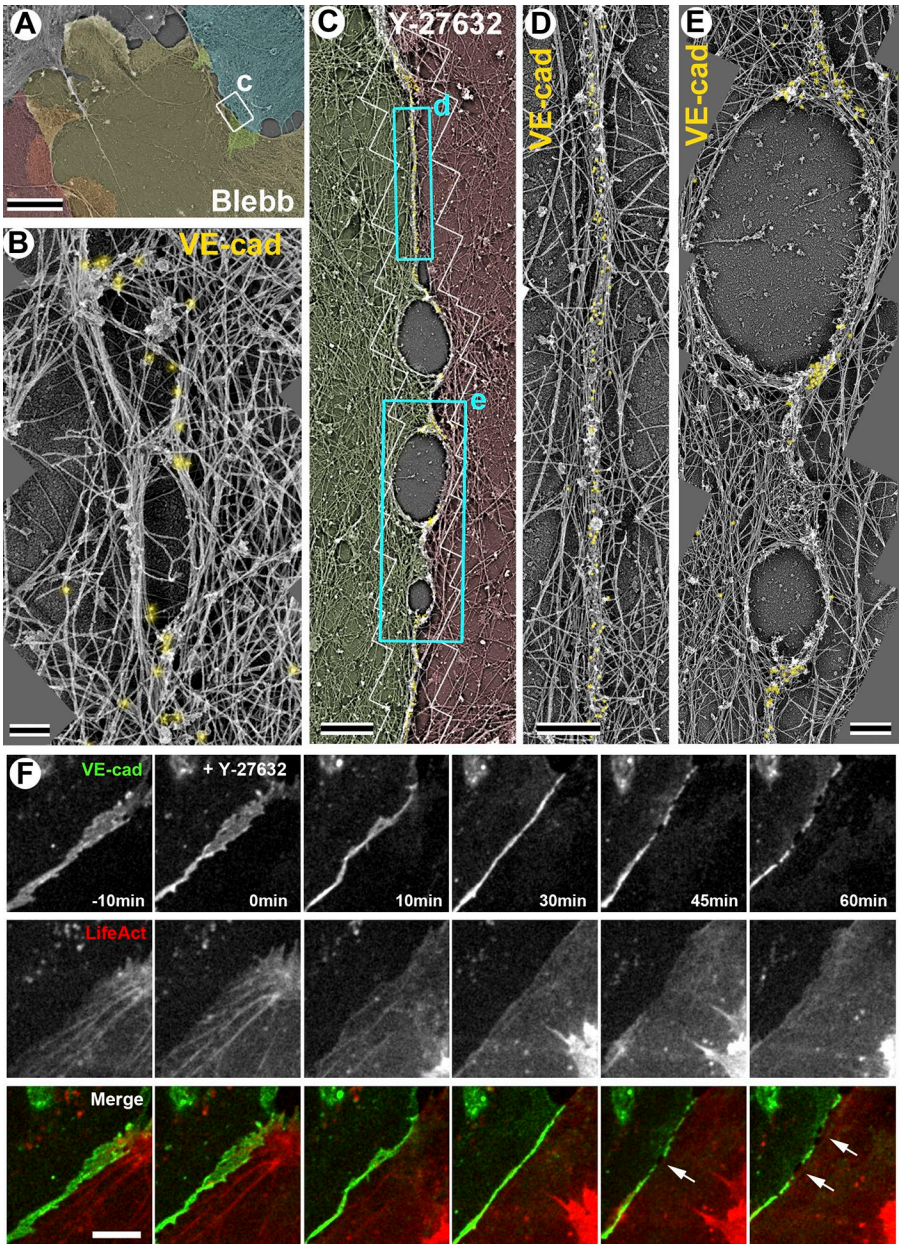

Figure 9. **Direct and indirect inhibition of NMII leads to expansion of lamellipodial overlaps and separation of linear AJs. (A and B)** Treatment of cells with 50 µM blebbistatin for 1 h. **(A)** A field of view with pseudocolored individual cells and cell overlaps. The boxed region is enlarged in B. **(B)** VE-cadherin immunogold (18 nm, yellow) labels cell–cell contacts but not gap edges. **(C–E)** Treatment of cells with 50 µM Y27632 for 1 h. **(C)** VE-cadherin immunogold (18 nm, yellow) at a linear AJ with gaps. Regions outlined in cyan are enlarged in D and E. **(D)** A preserved linear AJ is evenly labeled with VE-cadherin immunogold. **(E)** Oval gaps in the linear AJ have VE-cadherin only at remaining cell–cell junctions but not at gap edges. **(F)** Time-lapse sequences of GFP–VE-cadherin (green) and mCherry-LifeAct (red) at AJs in the course of Y-27632 treatment. Y-27632 was added at time 0. Arrows mark Y-27632–induced intercellular gaps. Bars: (A) 5 µm; (B) 200 nm; (C) 2 µm; (D and E) 500 nm; (F) 10 µm.

inhibitor Y-27632 (Fig. 9, C–E; and Fig. S9), which prevents ROCK-mediated activation of NMII. Both inhibitors produced roughly similar phenotypes. Their most obvious effect was a significant reduction of actin bundles and formation of prominent overlapping lamellipodia at cell–cell junctions. Some lamellipodia formed a ruffle above the neighboring cell. More commonly, a lamellipodium of one cell extended underneath a nondynamic (lacking lamellipodia) edge of the neighboring cell (Figs. 9 A and S9 A). Both types of cell–cell overlaps exhibited sparse VE-cadherin labeling. Local accumulations of VE-cadherin were seen only in cases when both cells formed small colliding lamellipodia (Fig. S9 C) or when one cell formed a small lamellipodium that collided with an actin bundle in the other cell (Fig. S9 B).

Some linear AJs in blebbistatin- (Fig. 9, A and B) or Y27632-treated (Fig. 9, C–E) cells were partially preserved, but often exhibited round or oval-shaped gaps. The preserved segments of linear AJs (Fig. 9 D) were flanked with thin tangential actin bundles and contained branched actin networks decorated by VE-cadherin immunogold (71.2 ± 14.5% of gold particles on branched networks and 28.8 ± 14.5% on loose unbranched

filaments). Oblique actin bundles as well as local VE-cadherin enrichments were mostly lost as expected after inhibition of NMII activity. In contrast with gaps generated by CK666 treatment, VE-cadherin immunogold did not label the edges of oval gaps in cells treated with blebbistatin (Fig. 9 B) or Y-27632 (Fig. 9 E) but was concentrated at the sites where cell edges preserved interaction (Fig. 9, B, D, and E).

Live-cell imaging of GFP–VE-cadherin and mCherry-LifeAct showed that shortly after Y-27632 addition, punctate and reticular AJs acquired linear morphology, with GFP–VE-cadherin forming a thin sharp line. Over time, gaps began to interrupt this linear VE-cadherin distribution (Fig. 9 F, Video 7, and control Video 6), thus recapitulating the phenotype observed by PREM.

Discussion

In this study, we answer two important outstanding questions regarding organization and functions of the actin cytoskeleton at AJs in endothelial cells. First, we show that VE-cadherin–containing adhesion complexes predominantly interact with Arp2/3-containing branched actin networks, whereas NMII-containing contractile actin bundles are located more distally and often interact with AJs via branched networks. These findings significantly change the common thinking that cadherin complexes directly interact with contractile actin arrays. Second, we demonstrate that branched actin networks function at mature AJs and are necessary for their maintenance, whereas branched actin was previously thought to function only during establishment and expansion of AJs (see Introduction). We propose that branched actin networks of contacting cells push against each other to maintain transinteraction of VE-cadherins. Our data also provide additional insights into interplay between pushing and pulling forces at AJs.

The major challenge for understanding relative roles of protrusion and contraction at AJs was spatial limitations imposed by AJ geometry, which confines both actin cytoskeleton activities to a very tight space. To solve this technical problem, we took advantage of unique features of PREM (Svitkina, 2017). First, because of single-filament resolution and preservation of the sample three-dimensionality, PREM can discriminate structural features of protrusive and contractile actin filament arrays. Second, PREM is easily compatible with immunochemistry and thus can precisely localize specific proteins. In this study, we used VE-cadherin as a reporter of AJs, NMIIA as a marker of contractile actin structures and Arpc2 or cortactin as markers of Arp2/3 complex–dependent protrusions.

In all AJ types examined in this study, VE-cadherin was mostly associated with the branched actin network, whereas more distal actin-NMII bundles were linked to VE-cadherin–rich regions through these branched networks. Although VE-cadherin binds actin filaments indirectly, the length of the bridge formed by adapter proteins (30 nm maximum; Bertocchi et al., 2017) is insufficient to cross the observed distances between VE-cadherin and actin-NMII bundles. However, it does not mean that VE-cadherin is unable to bind actin bundles because a fraction of VE-cadherin immunogold is found on tips of oblique bundles in linear AJs, but rather suggests that branched actin networks preferentially interact with VE-cadherin–catenin complexes.

Although the mutual arrangement of pushing and pulling actin arrays varies among AJ types (Fig. 10), it can be viewed as a continuum. In the most classic-looking linear AJs (Fig. 10 A), two tangential actin-NMII bundles closely flank a narrow strip of the branched network formed by two colliding subsets with VE-cadherin at their interface. In a modified version of linear AJs (Fig. 10 B), tangential bundles are located at a distance from the VE-cadherin–positive branched strip, but connected to the strip by oblique actin-NMII bundles or individual filaments. VE-cadherin is continuously distributed in these linear AJs, but it is also enriched at the sites of oblique bundle attachment, probably because of mechanical stimulation transmitted by these bundles. Similar cadherin clusters were detected in linear AJs by subdiffraction fluorescence microscopy (Indra et al., 2013; Truong Quang et al., 2013; Strale et al., 2015; Wu et al., 2015).

Among punctate AJ types, focal AJs (Fig. 10 D) most closely resemble linear AJs. At focal AJs, cell edges contact each other over significant distance despite discontinuous VE-cadherin distribution. Focal AJs could be formed from linear AJs through greater clustering and subsequent individualization of local VE-cadherin accumulations at the tips of oblique bundles. In turn, intercellular bridges (Fig. 10, E and F) closely resemble focal AJs except that the cell edges between bridges are retracted and form gaps. Branched actin networks in intercellular bridges can be present at the tips (Fig. 10 E) or along the length (Fig. 10 F) of filopodium-like protrusions. The engulfed fingers (Fig. 10 C) are likely formed from intercellular bridges, when one of the contacting cells resumes lamellipodial protrusion and runs over the bridge.

The apparent structural continuity among different AJs is consistent with the known ability of cells to interconvert AJs during their remodeling. We suggest that the whole range of observed AJ morphologies (Fig. 10) depends on a balance between the pushing force, which is generated by junctional branched networks along the length of the cell–cell contact, and the pulling force, which is produced by actin-NMII bundles. If cell contractility is reduced, the surviving AJs have morphology of linear AJs with sparse homogeneous VE-cadherin distribution as observed in this study and previously (Krendel et al., 1999; Sahai and Marshall, 2002; Shewan et al., 2005; Ayollo et al., 2009; Huveneers et al., 2012). Conversely, excessive contractility disrupts linear AJs and promotes focal AJs and intercellular bridges (Essler et al., 1998; Krendel et al., 1999; Gavard and Gutkind, 2008; Millán et al., 2010; Huveneers et al., 2012).

The consistent presence of branched actin networks at the VE-cadherin–positive AJs suggests important functional implications. We propose that branched actin networks of two cells constantly push against each other at the AJ in order to maintain transinteraction between VE-cadherins of contacting cells. Consistent with this idea, inhibition of Arp2/3 complex causes cell–cell separation, indicating that cells are unable to maintain AJs in these conditions probably because of the absence of adequate pushing forces from both cells. Arp2/3 inhibition may also act indirectly, for example, by up-regulating RhoA signaling and cell contractility (Korobova and Svitkina, 2008), which might explain the fast mode of cell–cell separation under

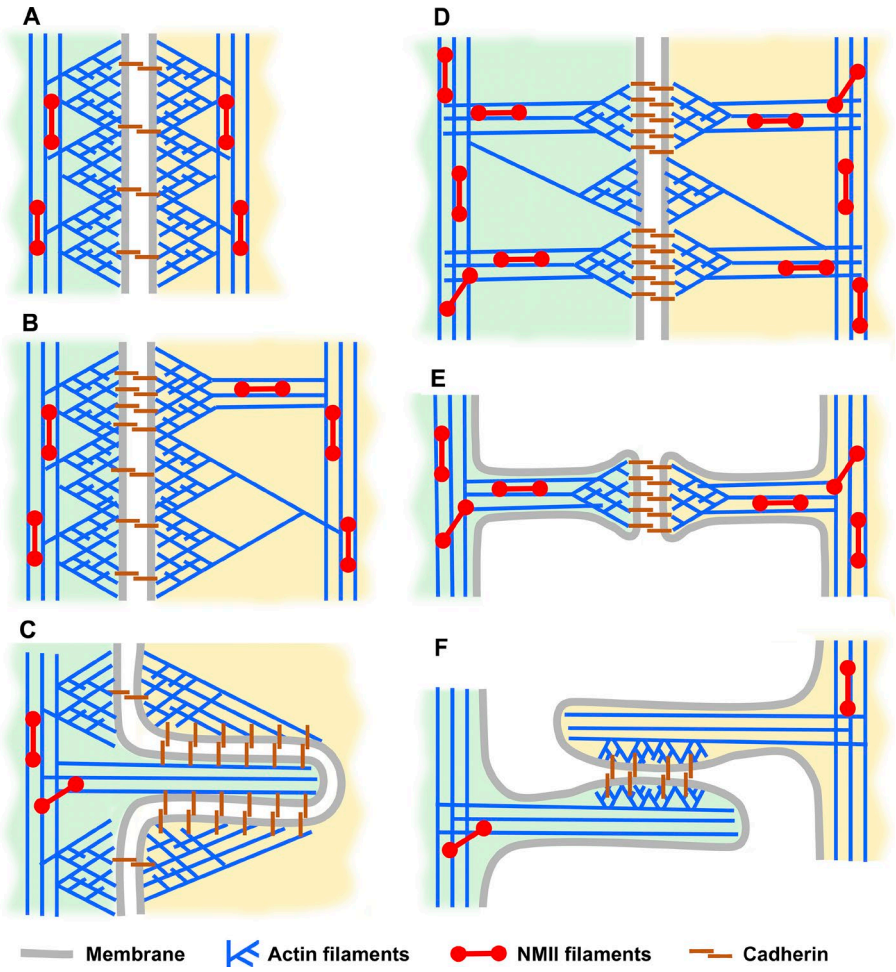

Figure 10. **Schematics of actin cytoskeleton organization at different types of AJs. (A)** Classic linear AJ. **(B)** Linear AJ with VE-cadherin enrichment at the tip of an oblique actin-NMII bundle. **(C)** Engulfed finger. **(D)** Focal AJs. **(E and F)** Intercellular bridges with tip-to-tip (E) or lateral (F) contacts.

CK666 treatment. The transient presence of VE-cadherin at the gap edges in CK666-treated cells is unusual because unengaged cadherin is normally endocytosed (Le et al., 1999) and becomes detergent soluble. Thus, inhibition of the Arp2/3 complex does not immediately disrupt the interaction of VE-cadherin with the cytoskeleton but leads to cell–cell separation through a different mechanism, most likely by compromising cadherin transinteraction in the intercellular space.

The branched junctional strip is distinct from the junctional lamellipodia, which repair intercellular gaps (Martinelli et al., 2013; Abu Taha et al., 2014). In our samples, the overlapping junctional lamellipodia show low VE-cadherin labeling and most likely function in establishing rather than maintaining AJs, in contrast with the branched junctional strip. The narrowness of the junctional strip may result from an interplay between two opposite processes induced by cadherin engagement: Arp2/3 complex–dependent protrusion (Kovacs et al., 2002; Helwani et al., 2004; Verma et al., 2004) and contact inhibition of protrusion (Abercrombie and Heaysman, 1954; Gloushankova et al., 1998; Kitt and Nelson, 2011).

NMII-mediated contractility is also important for AJ maintenance. Similar to previous studies (Shewan et al., 2005; Zhang et al., 2005; Smutny et al., 2010; Breyer et al., 2012), we found that inhibition of contractility leads to some loss of cadherins at AJs and formation of intercellular gaps. In contrast with Arp2/3 complex inhibition, we could not detect VE-cadherin at the gap edges after NMII inhibition, suggesting disassembly of cadherin complexes at the cytoplasmic face of the AJ, which makes cadherins susceptible to endocytosis and detergent extraction. A likely mechanism for cadherin complex disassembly is refolding of α-catenin into an autoinhibitory conformation in absence of force and subsequent uncoupling of VE-cadherin from the cytoskeleton.

In the absence of adequate structural data, it was previously assumed that contractile bundles are directly linked to the cadherin complexes (see Introduction). In this context, the linkage of oblique actin-NMII bundles to punctate AJs seems optimal for force transductions because it resembles stress fibers linked to focal adhesions. In contrast, the mechanism by which tangential bundles are linked to AJs and transmit force appeared much less obvious. Our findings that actin-NMII bundles are predominantly connected to VE-cadherin complexes at AJs by branched networks suggest that NMII-mediated contraction is transmitted to cadherin-based adhesion complexes through branched networks. With this geometry, orientation of actin filaments is optimal for efficient application of load to the adhesion complexes.

Indeed, it has been shown recently that vinculin forms a stronger catch bond with F-actin when force is directed toward the pointed end of the actin filament (Huang et al., 2017). Because most actin filaments in branched networks are oriented with their barbed ends to the membrane, they are optimally positioned to promote stronger attachment of adhesion complexes to the cytoskeleton.

If branched actin networks act as a force transmitter, they should be physically linked to contractile bundles. We indeed observed that branched networks frequently originate from actin filaments in tangential bundles, which thus serve as "mother" filaments for Arp2/3 complex–dependent nucleation. The "daughter" filaments that originate at an ∼70° angle from these mother filaments continue to branch further in the direction of the AJ, where they apparently make contacts with adhesion complexes. However, if contractile forces are transmitted to AJs by protrusive actin networks, the pushing and pulling forces are expected to cancel each other or at least diminish each other's contribution to AJ maintenance. A similar problem, however, also exists in lamellipodia. Lamellipodia use a branched actin network to generate protrusion and NMII-dependent contractility to stimulate retrograde flow and form cell–matrix adhesions. This analogy suggests existence of intricate regulation of contractile and protrusive forces at AJs, possibly through their alternation, similar to the oscillatory behavior of protrusion and contraction in lamellipodia (Giannone et al., 2004).

We also propose that besides generating contraction, tangential actin-NMII bundles can improve functionality of branched actin networks at AJs. First, these bundles help to initiate the junctional branched networks by supplying mother filaments for Arp2/3 complex–dependent nucleation. Second, they can serve as a stiff base that limits the retrograde flow of the branched network and thereby enhances the pushing force in the forward direction. Notably, retrograde flow still should exist because branched actin networks polymerize continuously but remain largely stationary in the context of AJs. The retrograde flow of the branched network in this narrow space can be an additional source of pulling force to stimulate adhesion at linear AJs. Finally, the tangential bundle can form a stiff barrier against which the branched network of the opposite cell exerts effective pressure in order to bring VE-cadherins of two cells within an interaction distance. This idea can potentially explain the unrestrained protrusion of overlapping lamellipodia and inefficient AJ formation after inhibition of cell contractility.

Although we conducted this study in endothelial cells, our conclusions can also apply to epithelial cells because molecular mechanisms of AJ formation are significantly conserved between two cell types and largely rely on different paralogs of the same protein families. However, there are also important differences between epithelial and endothelial cells. AJs in epithelial cells are more stable and uniform, whereas endothelial AJs are more dynamic. Epithelial AJs are associated with thicker tangential actin bundles that are thought to be positioned too close to each other to accommodate branched networks in between. Direct investigation of epithelial AJs is challenging because of extremely high density of their cytoskeleton. Future studies may advance our understanding of similarities and differences of the AJ cytoskeleton between endothelial and epithelial cells.

In conclusion, we show that Arp2/3 complex–dependent branched actin filament networks are an essential component of all types of AJs including mature linear AJs. Branched actin networks represent the actual actin cytoskeleton component that is linked to cadherin-based adhesion complexes. We propose that the key role of junctional branched networks is to push plasma membranes of contacting cells against each other and thus maintain transinteraction between cadherins. The contractile actin–NMII bundles that are associated with AJs mechanically stimulate assembly of adhesion complexes by generating pulling force that is transmitted to cadherins via branched actin networks. Additionally, tangential actin bundles serve as a launch pad for assembly of the junctional branched networks and as a structural base that restrains pushing force generated by the branched network and its retrograde flow within a narrow space. Our data provide an important conceptual framework to explain the results of functional experiments that target various components and regulators of different actin cytoskeleton subsets at AJs.

Materials and methods

Cells and reagents

HUVECs (CC-2519; Lonza) were cultured in endothelial cell basal medium (CC-3121; Lonza) with supplements (CC-4133; Lonza) and maintained for no longer than six passages. For experiments, HUVECs were plated on coverslips or glass-bottom dishes (MatTek Corporation) coated with ∼50 µg/ml (5 mg/cm^2) collagen from rat tail (354236; BD). Primary mouse monoclonal antibodies were used for cadherin-5 (VE-cadherin; 610251; BD), cortactin p80/85 (clone 4F11; 05-180; EMD Millipore), and NMIIA (ab55456; Abcam). Primary rabbit monoclonal antibody was used for VASP (clone 9A2; 3132; Cell Signaling Technology). Primary rabbit polyclonal antibodies were used for ArpC2 (p34-Arc; 07-227; EMD Millipore), α–E-catenin (3236T; Cell Signaling Technology), and NMIIA (BT-567; Biomedical Technologies). Secondary antibodies and phalloidin fluorescently labeled with Alexa Fluor 488, 594, and 680 were from Invitrogen; secondary anti–rabbit and anti–mouse IgG antibodies conjugated to 12- or 18-nm colloidal gold were from Jackson ImmunoResearch Laboratories, Inc. Blebbistatin (B592500; Toronto Research Chemicals) was prepared from 10-mM stock in DMSO, and Y-27632 (Y100500; Toronto Research Chemicals) was prepared from 10-mM stock in water. For fluorescence microscopy experiments, cells were treated with 50 µM blebbistatin or 50 µM Y-27632 in culture medium for 1 h and then processed for immunofluorescence or PREM. CK666 (SML0006; Sigma-Aldrich) was prepared from 10-mM stock in DMSO and used at a concentration of 100 µM for 40–60 min.

The following plasmids were used in live-cell imaging experiments: GFP–VE-cadherin in adenoviral vector (gift from Y. Komarova, University of Illinois, Chicago, IL) and mCherry-LifeAct in pLL-5.0 lentiviral vector (the vector is a gift from A. Efimov, Fox Chase Cancer Center, Philadelphia, PA; Chia et al., 2016). For lentivirus production, HEK293T cells were cultured in DMEM supplemented with 10% FBS for 24 h before transfection. Cultures at 50–70% confluence were transfected with a mixture of packaging (Pax2), envelope (MD2G), and transfer (pLL–mCherry-LifeAct)

plasmids using Fugene6 reagent (Promega). After incubation for 5–6 h with the transfection mixture, the medium was replaced with DMEM with 10% FBS. The medium containing viral particles was collected 48 h later. For infection, HUVECs were incubated for 5–6 h with the virus-containing medium supplemented with 8 µg/ml protamine sulfate (Sigma-Aldrich).

Fluorescence microscopy

Immunofluorescence staining of HUVECs was performed after simultaneous fixation and extraction with the mixture of 4% formaldehyde (15710; Electron Microscopy Sciences) and 0.3% Triton X-100 in PBS for 15 min. For cortactin staining, cells were extracted with 1% Triton X-100 in PEM buffer (100 mM piperazine-N,N′-bis(2-ethanesulfonic acid)-KOH, pH 6.9, 1 mM $MgCl_2$, and 1 mM EGTA) containing 2% polyethylene glycol (M_r 35,000), 5 µM phalloidin, and 2 µM taxol for 3 min. After washing with PEM buffer, extracted unfixed cells were incubated with the primary antibody, washed with the PEM buffer, and fixed with 0.2% glutaraldehyde. After quenching with 2 mg/ml $NaBH_4$ in PBS for 10 min, cells were stained with secondary Alexa Fluor antibody. Coverslips were mounted to slides with ProLong Gold antifade mountant (P36941; Molecular Probes). Light microscopy was performed using an Eclipse TE2000-U inverted microscope (Nikon) equipped with Plan Apochromat 20× 0.75-NA and Apochromat 100× 1.3-NA objectives and Cascade 512B CCD camera (Photometrics) driven by MetaMorph imaging software (Molecular Devices).

For live-cell imaging, cells were maintained at 37°C in humidified atmosphere with 5% CO_2 using an UNO stage-top incubator (Okolab) with 20–30 min allowed for cell accommodation before imaging. Time-lapse sequences were acquired every 10 s for 15 min (Video 1) or every 1 min for 60–70 min (Videos 2, 3, 4, 5, 6, and 7). Vehicle (DMSO for CK666 and culture medium for Y-27632) or drugs were added during a pause between the ninth and 10th frames at the same concentration as for experiments with fixed cells. Imaging was performed using an Eclipse T*i* inverted microscope (Nikon) equipped with a CSUX1 spinning disk (Yokogawa Electric Corporation), CFI60 Plan Apochromat Lambda 20× 0.75-NA and CFI60 Apochromat total internal reflection fluorescence 100× 1.49-NA oil immersion objectives, and a QuantEM 512SC digital camera (Photometrics) driven by NIS Elements software (Nikon). Multiple positioning in the x–y plane and single-slice spinning-disk confocal mode with 488- and 561-nm laser wavelengths and FITC and TRITC filters were used for imaging. FIJI software (ImageJ; National Institutes of Health) was used to adjust image contrast and create montages. Gaussian blur filter with 1-pixel radius was applied to Video 1 to reduce noise.

PREM

Sample preparation for regular and immunogold PREM was performed as described previously (Svitkina, 2007, 2016). In brief, cells were extracted as described for cortactin staining, washed with PEM, and fixed with 2% glutaraldehyde in 0.1 M Na-cacodylate, pH 7.3. Fixed cells were sequentially treated with 0.1% tannic acid and 0.2% uranyl acetate in water, critical-point dried, coated with platinum and carbon, and transferred onto EM grids for observation.

For immunogold staining, extracted unfixed cells were incubated for 30 min with a primary antibody in PEM buffer containing 5 µM unlabeled phalloidin and 2 µM taxol, washed with PEM buffer, and fixed with 0.2% glutaraldehyde. After quenching with 2 mg/ml $NaBH_4$ in PBS for 10 min, cells were blocked with 1% BSA in buffer A (20 mM Tris-HCl, pH 8, 0.5 M NaCl, and 0.05% Tween-20), stained with secondary colloidal gold–conjugated antibody, and postfixed with 2% glutaraldehyde.

Analyses and quantification of PREM data

PREM samples were analyzed using a JEM 1011 transmission electron microscope (JEOL) operated at 100 kV. Images were captured by an ORIUS 832.10W charge-coupled device camera (Gatan) and presented in inverted contrast. Stitching of PREM images was done using the Photomerge tool in Photoshop (Adobe) with the Reposition option. Automatic alignment of layers was manually corrected before applying the Auto-Blend Layers tool. Identification of gold particles in PREM samples was performed at high magnification after contrast enhancement to distinguish them from other bright objects in the samples such as actin filament tips. Color labeling was performed using Photoshop as described previously (Shutova et al., 2012). In brief, gold particles were highlighted using the Brush tool in Photoshop with 50% opacity. Pseudocolors were applied using the Hue/Saturation tool in Photoshop to avoid obscuring the structural details.

For quantification of branch orientation relative to VE-cadherin distribution in linear AJs, actin filament branches were identified and colorized at high magnification to distinguish branches from filament intersections or separating filament pairs. Branch orientation was scored according to three categories—toward, away, or parallel to a line drawn through middle of the VE-cadherin–labeled zone—and expressed as a percentage of all detected branches. For quantification of gold labeling of different actin structures, gold particles were categorized as bound to branched actin networks or unbranched actin filaments, either bundled or unbundled. For quantification of VE-cadherin and Arpc2 immunogold colocalization, 12- and 18-nm gold particles were scored within the visually recognizable junctional branched networks at linear AJs and separately in the rest of the image. Densities of each label were determined by per-unit area occupied by the cytoskeleton in respective cell regions. The area covered by the cytoskeleton was determined using FIJI software by thresholding after increasing the image contrast between the cytoskeleton and the background and applying a mean filter of 20 pixels (~10 nm) to reduce granularity of the background. Statistical significance was determined by Tukey–Kramer multiple comparisons test after evaluating data distribution normality by Kolmogorov–Smirnov normality test using Instat software (GraphPad Software).

Online supplemental material

Fig. S1 shows the cytoskeleton of linear AJs associated with tangential and/or oblique actin-NMII bundles. Fig. S2 shows high magnification of gold particles and VE-cadherin immunogold labeling of cell–cell contacts made by overlapping lamellipodia. Fig. S3 shows immunofluorescence and immunogold labeling of AJs with α-catenin antibody. Fig. S4 shows immunofluorescence

and immunogold staining of VE-cadherin in confluent HUVEC monolayers. Fig. S5 shows orientation of branched actin filaments at linear AJs. Fig. S6 shows branched actin networks in intercellular bridges. Fig. S7 shows reticular AJs. Fig. S8 shows cortactin immunostaining of control and CK666-treated HUVECs. Fig. S9 shows AJs after treatment with Y27632. Video 1 shows dynamics of GFP–VE-cadherin and mCherry-LifeAct at linear AJs. Videos 2, 3, 4, 5, 6, and 7 show dynamics of AJs after addition of DMSO (Video 2), CK666 (Videos 3, 4, and 5), culture medium (Video 6), or Y-27632 (Video 7).

Acknowledgments

We thank Dr. Yulia Komarova for the gift of GFP–VE-cadherin construct and Dr. Andrey Efimov for pLL-mCherry vector.

This work was supported by National Institutes of Health grant R01 GM 095977 to T.M. Svitkina.

The authors declare no competing financial interests.

Author contributions: N. Efimova and T.M. Svitkina conceived the project, designed research, performed experiments, analyzed the data, and wrote the paper.

Submitted: 15 August 2017
Revised: 21 December 2017
Accepted: 12 February 2018

References

Abercrombie, M., and J.E. Heaysman. 1954. Observations on the social behaviour of cells in tissue culture. II. Monolayering of fibroblasts. *Exp. Cell Res.* 6:293–306. https://doi.org/10.1016/0014-4827(54)90176-7

Abu Taha, A., M. Taha, J. Seebach, and H.J. Schnittler. 2014. ARP2/3-mediated junction-associated lamellipodia control VE-cadherin-based cell junction dynamics and maintain monolayer integrity. *Mol. Biol. Cell.* 25:245–256. https://doi.org/10.1091/mbc.E13-07-0404

Adams, C.L., Y.T. Chen, S.J. Smith, and W.J. Nelson. 1998. Mechanisms of epithelial cell-cell adhesion and cell compaction revealed by high-resolution tracking of E-cadherin-green fluorescent protein. *J. Cell Biol.* 142:1105–1119. https://doi.org/10.1083/jcb.142.4.1105

Ayollo, D.V., I.Y. Zhitnyak, J.M. Vasiliev, and N.A. Gloushankova. 2009. Rearrangements of the actin cytoskeleton and E-cadherin-based adherens junctions caused by neoplastic transformation change cell-cell interactions. *PLoS One.* 4:e8027. https://doi.org/10.1371/journal.pone.0008027

Barry, A.K., H. Tabdili, I. Muhamed, J. Wu, N. Shashikanth, G.A. Gomez, A.S. Yap, C.J. Gottardi, J. de Rooij, N. Wang, and D.E. Leckband. 2014. α-catenin cytomechanics—Role in cadherin-dependent adhesion and mechanotransduction. *J. Cell Sci.* 127:1779–1791. https://doi.org/10.1242/jcs.139014

Bertocchi, C., Y. Wang, A. Ravasio, Y. Hara, Y. Wu, T. Sailov, M.A. Baird, M.W. Davidson, R. Zaidel-Bar, Y. Toyama, et al. 2017. Nanoscale architecture of cadherin-based cell adhesions. *Nat. Cell Biol.* 19:28–37. https://doi.org/10.1038/ncb3456

Bieling, P., T.D. Li, J. Weichsel, R. McGorty, P. Jreij, B. Huang, D.A. Fletcher, and R.D. Mullins. 2016. Force feedback controls motor activity and mechanical properties of self-assembling branched actin networks. *Cell.* 164:115–127. https://doi.org/10.1016/j.cell.2015.11.057

Breyer, J., J. Samarin, M. Rehm, L. Lautscham, B. Fabry, and M. Goppelt-Struebe. 2012. Inhibition of Rho kinases increases directional motility of microvascular endothelial cells. *Biochem. Pharmacol.* 83:616–626. https://doi.org/10.1016/j.bcp.2011.12.012

Buckley, C.D., J. Tan, K.L. Anderson, D. Hanein, N. Volkmann, W.I. Weis, W.J. Nelson, and A.R. Dunn. 2014. Cell adhesion. The minimal cadherin-catenin complex binds to actin filaments under force. *Science.* 346:1254211. https://doi.org/10.1126/science.1254211

Cain, R.J., B. Vanhaesebroeck, and A.J. Ridley. 2010. The PI3K p110α isoform regulates endothelial adherens junctions via Pyk2 and Rac1. *J. Cell Biol.* 188:863–876. https://doi.org/10.1083/jcb.200907135

Cameron, L.A., T.M. Svitkina, D. Vignjevic, J.A. Theriot, and G.G. Borisy. 2001. Dendritic organization of actin comet tails. *Curr. Biol.* 11:130–135. https://doi.org/10.1016/S0960-9822(01)00022-7

Chen, C.S., S. Hong, I. Indra, A.P. Sergeeva, R.B. Troyanovsky, L. Shapiro, B. Honig, and S.M. Troyanovsky. 2015. α-Catenin–mediated cadherin clustering couples cadherin and actin dynamics. *J. Cell Biol.* 210:647–661. https://doi.org/10.1083/jcb.201412064

Chia, J.X., N. Efimova, and T.M. Svitkina. 2016. Neurite outgrowth is driven by actin polymerization even in the presence of actin polymerization inhibitors. *Mol. Biol. Cell.* 27:3695–3704. https://doi.org/10.1091/mbc.E16-04-0253

Cojoc, D., F. Difato, E. Ferrari, R.B. Shahapure, J. Laishram, M. Righi, E.M. Di Fabrizio, and V. Torre. 2007. Properties of the force exerted by filopodia and lamellipodia and the involvement of cytoskeletal components. *PLoS One.* 2:e1072. https://doi.org/10.1371/journal.pone.0001072

Collins, A., A. Warrington, K.A. Taylor, and T. Svitkina. 2011. Structural organization of the actin cytoskeleton at sites of clathrin-mediated endocytosis. *Curr. Biol.* 21:1167–1175. https://doi.org/10.1016/j.cub.2011.05.048

Dejana, E., and C. Giampietro. 2012. Vascular endothelial-cadherin and vascular stability. *Curr. Opin. Hematol.* 19:218–223. https://doi.org/10.1097/MOH.0b013e3283523e1c

Dominguez, R. 2009. Actin filament nucleation and elongation factors—Structure-function relationships. *Crit. Rev. Biochem. Mol. Biol.* 44:351–366. https://doi.org/10.3109/10409230903277340

Ehrlich, J.S., M.D. Hansen, and W.J. Nelson. 2002. Spatio-temporal regulation of Rac1 localization and lamellipodia dynamics during epithelial cell-cell adhesion. *Dev. Cell.* 3:259–270. https://doi.org/10.1016/S1534-5807(02)00216-2

Essler, M., M. Amano, H.J. Kruse, K. Kaibuchi, P.C. Weber, and M. Aepfelbacher. 1998. Thrombin inactivates myosin light chain phosphatase via Rho and its target Rho kinase in human endothelial cells. *J. Biol. Chem.* 273:21867–21874. https://doi.org/10.1074/jbc.273.34.21867

Furman, C., A.L. Sieminski, A.V. Kwiatkowski, D.A. Rubinson, E. Vasile, R.T. Bronson, R. Fässler, and F.B. Gertler. 2007. Ena/VASP is required for endothelial barrier function in vivo. *J. Cell Biol.* 179:761–775. https://doi.org/10.1083/jcb.200705002

Gates, J., J.P. Mahaffey, S.L. Rogers, M. Emerson, E.M. Rogers, S.L. Sottile, D. Van Vactor, F.B. Gertler, and M. Peifer. 2007. Enabled plays key roles in embryonic epithelial morphogenesis in Drosophila. *Development.* 134:2027–2039. https://doi.org/10.1242/dev.02849

Gavard, J., and J.S. Gutkind. 2008. Protein kinase C-related kinase and ROCK are required for thrombin-induced endothelial cell permeability downstream from Galpha12/13 and Galpha11/q. *J. Biol. Chem.* 283:29888–29896. https://doi.org/10.1074/jbc.M803880200

Giannone, G., B.J. Dubin-Thaler, H.G. Döbereiner, N. Kieffer, A.R. Bresnick, and M.P. Sheetz. 2004. Periodic lamellipodial contractions correlate with rearward actin waves. *Cell.* 116:431–443. https://doi.org/10.1016/S0092-8674(04)00058-3

Giannotta, M., M. Trani, and E. Dejana. 2013. VE-cadherin and endothelial adherens junctions: Active guardians of vascular integrity. *Dev. Cell.* 26:441–454. https://doi.org/10.1016/j.devcel.2013.08.020

Gloushankova, N.A., M.F. Krendel, N.O. Alieva, E.M. Bonder, H.H. Feder, J.M. Vasiliev, and I.M. Gelfand. 1998. Dynamics of contacts between lamellae of fibroblasts: Essential role of the actin cytoskeleton. *Proc. Natl. Acad. Sci. USA.* 95:4362–4367. https://doi.org/10.1073/pnas.95.8.4362

Hayer, A., L. Shao, M. Chung, L.M. Joubert, H.W. Yang, F.C. Tsai, A. Bisaria, E. Betzig, and T. Meyer. 2016. Engulfed cadherin fingers are polarized junctional structures between collectively migrating endothelial cells. *Nat. Cell Biol.* 18:1311–1323. https://doi.org/10.1038/ncb3438

Helwani, F.M., E.M. Kovacs, A.D. Paterson, S. Verma, R.G. Ali, A.S. Fanning, S.A. Weed, and A.S. Yap. 2004. Cortactin is necessary for E-cadherin–mediated contact formation and actin reorganization. *J. Cell Biol.* 164:899–910. https://doi.org/10.1083/jcb.200309034

Hirokawa, N., and L.G. Tilney. 1982. Interactions between actin filaments and between actin filaments and membranes in quick-frozen and deeply etched hair cells of the chick ear. *J. Cell Biol.* 95:249–261. https://doi.org/10.1083/jcb.95.1.249

Hoelzle, M.K., and T. Svitkina. 2012. The cytoskeletal mechanisms of cell-cell junction formation in endothelial cells. *Mol. Biol. Cell.* 23:310–323. https://doi.org/10.1091/mbc.E11-08-0719

Hoffman, B.D., and A.S. Yap. 2015. Towards a dynamic understanding of cadherin-based mechanobiology. *Trends Cell Biol.* 25:803–814. https://doi.org/10.1016/j.tcb.2015.09.008

Huang, D.L., N.A. Bax, C.D. Buckley, W.I. Weis, and A.R. Dunn. 2017. Vinculin forms a directionally asymmetric catch bond with F-actin. *Science.* 357:703–706. https://doi.org/10.1126/science.aan2556

Hull, B.E., and L.A. Staehelin. 1979. The terminal web. A reevaluation of its structure and function. *J. Cell Biol.* 81:67–82. https://doi.org/10.1083/jcb.81.1.67

Huveneers, S., and J. de Rooij. 2013. Mechanosensitive systems at the cadherin-F-actin interface. *J. Cell Sci.* 126:403–413. https://doi.org/10.1242/jcs.109447

Huveneers, S., J. Oldenburg, E. Spanjaard, G. van der Krogt, I. Grigoriev, A. Akhmanova, H. Rehmann, and J. de Rooij. 2012. Vinculin associates with endothelial VE-cadherin junctions to control force-dependent remodeling. *J. Cell Biol.* 196:641–652. https://doi.org/10.1083/jcb.201108120

Indra, I., S. Hong, R. Troyanovsky, B. Kormos, and S. Troyanovsky. 2013. The adherens junction: A mosaic of cadherin and nectin clusters bundled by actin filaments. *J. Invest. Dermatol.* 133:2546–2554. https://doi.org/10.1038/jid.2013.200

Ivanov, A.I., D. Hunt, M. Utech, A. Nusrat, and C.A. Parkos. 2005. Differential roles for actin polymerization and a myosin II motor in assembly of the epithelial apical junctional complex. *Mol. Biol. Cell.* 16:2636–2650. https://doi.org/10.1091/mbc.E05-01-0043

Kitt, K.N., and W.J. Nelson. 2011. Rapid suppression of activated Rac1 by cadherins and nectins during de novo cell-cell adhesion. *PLoS One.* 6:e17841. https://doi.org/10.1371/journal.pone.0017841

Korobova, F., and T. Svitkina. 2008. Arp2/3 complex is important for filopodia formation, growth cone motility, and neuritogenesis in neuronal cells. *Mol. Biol. Cell.* 19:1561–1574. https://doi.org/10.1091/mbc.E07-09-0964

Korobova, F., and T. Svitkina. 2010. Molecular architecture of synaptic actin cytoskeleton in hippocampal neurons reveals a mechanism of dendritic spine morphogenesis. *Mol. Biol. Cell.* 21:165–176. https://doi.org/10.1091/mbc.E09-07-0596

Kovacs, E.M., M. Goodwin, R.G. Ali, A.D. Paterson, and A.S. Yap. 2002. Cadherin-directed actin assembly: E-cadherin physically associates with the Arp2/3 complex to direct actin assembly in nascent adhesive contacts. *Curr. Biol.* 12:379–382. https://doi.org/10.1016/S0960-9822(02)00661-9

Kovacs, E.M., S. Verma, R.G. Ali, A. Ratheesh, N.A. Hamilton, A. Akhmanova, and A.S. Yap. 2011. N-WASP regulates the epithelial junctional actin cytoskeleton through a non-canonical post-nucleation pathway. *Nat. Cell Biol.* 13:934–943. https://doi.org/10.1038/ncb2290

Krendel, M.F., and E.M. Bonder. 1999. Analysis of actin filament bundle dynamics during contact formation in live epithelial cells. *Cell Motil. Cytoskeleton.* 43:296–309. https://doi.org/10.1002/(SICI)1097-0169(1999)43:4%3C296::AID-CM3%3E3.0.CO;2-U

Krendel, M., N.A. Gloushankova, E.M. Bonder, H.H. Feder, J.M. Vasiliev, and I.M. Gelfand. 1999. Myosin-dependent contractile activity of the actin cytoskeleton modulates the spatial organization of cell-cell contacts in cultured epitheliocytes. *Proc. Natl. Acad. Sci. USA.* 96:9666–9670. https://doi.org/10.1073/pnas.96.17.9666

Ladoux, B., W.J. Nelson, J. Yan, and R.M. Mège. 2015. The mechanotransduction machinery at work at adherens junctions. *Integr. Biol.* 7:1109–1119. https://doi.org/10.1039/C5IB00070J

Le, T.L., A.S. Yap, and J.L. Stow. 1999. Recycling of E-cadherin: A potential mechanism for regulating cadherin dynamics. *J. Cell Biol.* 146:219–232.

Lee, N.K., K.W. Fok, A. White, N.H. Wilson, C.J. O'Leary, H.L. Cox, M. Michael, A.S. Yap, and H.M. Cooper. 2016. Neogenin recruitment of the WAVE regulatory complex maintains adherens junction stability and tension. *Nat. Commun.* 7:11082. https://doi.org/10.1038/ncomms11082

Liu, Z., J.L. Tan, D.M. Cohen, M.T. Yang, N.J. Sniadecki, S.A. Ruiz, C.M. Nelson, and C.S. Chen. 2010. Mechanical tugging force regulates the size of cell-cell junctions. *Proc. Natl. Acad. Sci. USA.* 107:9944–9949. https://doi.org/10.1073/pnas.0914547107

Martinelli, R., M. Kamei, P.T. Sage, R. Massol, L. Varghese, T. Sciuto, M. Toporsian, A.M. Dvorak, T. Kirchhausen, T.A. Springer, and C.V. Carman. 2013. Release of cellular tension signals self-restorative ventral lamellipodia to heal barrier micro-wounds. *J. Cell Biol.* 201:449–465. https://doi.org/10.1083/jcb.201209077

Mège, R.M., and N. Ishiyama. 2017. Integration of cadherin adhesion and cytoskeleton at adherens junctions. *Cold Spring Harb. Perspect. Biol.* 9:a028738. https://doi.org/10.1101/cshperspect.a028738

Mège, R.M., J. Gavard, and M. Lambert. 2006. Regulation of cell-cell junctions by the cytoskeleton. *Curr. Opin. Cell Biol.* 18:541–548. https://doi.org/10.1016/j.ceb.2006.08.004

Michael, M., and A.S. Yap. 2013. The regulation and functional impact of actin assembly at cadherin cell-cell adhesions. *Semin. Cell Dev. Biol.* 24:298–307. https://doi.org/10.1016/j.semcdb.2012.12.004

Millán, J., R.J. Cain, N. Reglero-Real, C. Bigarella, B. Marcos-Ramiro, L. Fernández-Martín, I. Correas, and A.J. Ridley. 2010. Adherens junctions connect stress fibres between adjacent endothelial cells. *BMC Biol.* 8:11. https://doi.org/10.1186/1741-7007-8-11

Naydenov, N.G., A. Feygin, D. Wang, J.F. Kuemmerle, G. Harris, M.A. Conti, R.S. Adelstein, and A.I. Ivanov. 2016. Nonmuscle myosin IIA regulates intestinal epithelial barrier in vivo and plays a protective role during experimental colitis. *Sci. Rep.* 6:24161. https://doi.org/10.1038/srep24161

Oldenburg, J., G. van der Krogt, F. Twiss, A. Bongaarts, Y. Habani, J.A. Slotman, A. Houtsmuller, S. Huveneers, and J. de Rooij. 2015. VASP, zyxin and TES are tension-dependent members of Focal Adherens Junctions independent of the α-catenin-vinculin module. *Sci. Rep.* 5:17225. https://doi.org/10.1038/srep17225

Padmanabhan, A., M.V. Rao, Y. Wu, and R. Zaidel-Bar. 2015. Jack of all trades: Functional modularity in the adherens junction. *Curr. Opin. Cell Biol.* 36:32–40. https://doi.org/10.1016/j.ceb.2015.06.008

Pollard, T.D. 2007. Regulation of actin filament assembly by Arp2/3 complex and formins. *Annu. Rev. Biophys. Biomol. Struct.* 36:451–477. https://doi.org/10.1146/annurev.biophys.35.040405.101936

Reinhard, M., M. Halbrügge, U. Scheer, C. Wiegand, B.M. Jockusch, and U. Walter. 1992. The 46/50 kDa phosphoprotein VASP purified from human platelets is a novel protein associated with actin filaments and focal contacts. *EMBO J.* 11:2063–2070.

Röper, K. 2015. Integration of cell-cell adhesion and contractile actomyosin activity during morphogenesis. *Curr. Top. Dev. Biol.* 112:103–127. https://doi.org/10.1016/bs.ctdb.2014.11.017

Rottner, K., B. Behrendt, J.V. Small, and J. Wehland. 1999. VASP dynamics during lamellipodia protrusion. *Nat. Cell Biol.* 1:321–322. https://doi.org/10.1038/13040

Ryu, J.R., A. Echarri, R. Li, and A.M. Pendergast. 2009. Regulation of cell-cell adhesion by Abi/Diaphanous complexes. *Mol. Cell. Biol.* 29:1735–1748. https://doi.org/10.1128/MCB.01483-08

Sahai, E., and C.J. Marshall. 2002. ROCK and Dia have opposing effects on adherens junctions downstream of Rho. *Nat. Cell Biol.* 4:408–415. https://doi.org/10.1038/ncb796

Sanger, J.M., and J.W. Sanger. 1980. Banding and polarity of actin filaments in interphase and cleaving cells. *J. Cell Biol.* 86:568–575. https://doi.org/10.1083/jcb.86.2.568

Schnittler, H., M. Taha, M.O. Schnittler, A.A. Taha, N. Lindemann, and J. Seebach. 2014. Actin filament dynamics and endothelial cell junctions: The Ying and Yang between stabilization and motion. *Cell Tissue Res.* 355:529–543. https://doi.org/10.1007/s00441-014-1856-2

Seebach, J., A.A. Taha, J. Lenk, N. Lindemann, X. Jiang, K. Brinkmann, S. Bogdan, and H.J. Schnittler. 2015. The CellBorderTracker, a novel tool to quantitatively analyze spatiotemporal endothelial junction dynamics at the subcellular level. *Histochem. Cell Biol.* 144:517–532. https://doi.org/10.1007/s00418-015-1357-8

Shewan, A.M., M. Maddugoda, A. Kraemer, S.J. Stehbens, S. Verma, E.M. Kovacs, and A.S. Yap. 2005. Myosin 2 is a key Rho kinase target necessary for the local concentration of E-cadherin at cell-cell contacts. *Mol. Biol. Cell.* 16:4531–4542. https://doi.org/10.1091/mbc.E05-04-0330

Shutova, M., C. Yang, J.M. Vasiliev, and T. Svitkina. 2012. Functions of nonmuscle myosin II in assembly of the cellular contractile system. *PLoS One.* 7:e40814. https://doi.org/10.1371/journal.pone.0040814

Smutny, M., H.L. Cox, J.M. Leerberg, E.M. Kovacs, M.A. Conti, C. Ferguson, N.A. Hamilton, R.G. Parton, R.S. Adelstein, and A.S. Yap. 2010. Myosin II isoforms identify distinct functional modules that support integrity of the epithelial zonula adherens. *Nat. Cell Biol.* 12:696–702. https://doi.org/10.1038/ncb2072

Strale, P.O., L. Duchesne, G. Peyret, L. Montel, T. Nguyen, E. Png, R. Tampé, S. Troyanovsky, S. Hénon, B. Ladoux, and R.M. Mège. 2015. The formation of ordered nanoclusters controls cadherin anchoring to actin and cell-cell contact fluidity. *J. Cell Biol.* 210:333–346. https://doi.org/10.1083/jcb.201410111

Svitkina, T. 2007. Electron microscopic analysis of the leading edge in migrating cells. *Methods Cell Biol.* 79:295–319. https://doi.org/10.1016/S0091-679X(06)79012-4

Svitkina, T.M. 2013. Ultrastructure of protrusive actin filament arrays. *Curr. Opin. Cell Biol.* 25:574–581. https://doi.org/10.1016/j.ceb.2013.04.003

Svitkina, T. 2016. Imaging cytoskeleton components by electron microscopy. *Methods Mol. Biol.* 1365:99–118. https://doi.org/10.1007/978-1-4939-3124-8_5

Svitkina, T.M. 2017. Platinum replica electron microscopy: Imaging the cytoskeleton globally and locally. *Int. J. Biochem. Cell Biol.* 86:37–41. https://doi.org/10.1016/j.biocel.2017.03.009

Svitkina, T. 2018. The actin cytoskeleton and actin-based motility. *Cold Spring Harb. Perspect. Biol.* 10:a018267. https://doi.org/10.1101/cshperspect.a018267

Svitkina, T.M., and G.G. Borisy. 1999. Arp2/3 complex and actin depolymerizing factor/cofilin in dendritic organization and treadmilling of actin filament array in lamellipodia. *J. Cell Biol.* 145:1009–1026. https://doi.org/10.1083/jcb.145.5.1009

Svitkina, T.M., A.B. Verkhovsky, and G.G. Borisy. 1995. Improved procedures for electron microscopic visualization of the cytoskeleton of cultured cells. *J. Struct. Biol.* 115:290–303. https://doi.org/10.1006/jsbi.1995.1054

Svitkina, T.M., A.B. Verkhovsky, K.M. McQuade, and G.G. Borisy. 1997. Analysis of the actin–myosin II system in fish epidermal keratocytes: Mechanism of cell body translocation. *J. Cell Biol.* 139:397–415. https://doi.org/10.1083/jcb.139.2.397

Tang, V.W., and W.M. Brieher. 2012. α-Actinin-4/FSGS1 is required for Arp2/3-dependent actin assembly at the adherens junction. *J. Cell Biol.* 196:115–130. https://doi.org/10.1083/jcb.201103116

Thomas, W.A., C. Boscher, Y.S. Chu, D. Cuvelier, C. Martinez-Rico, R. Seddiki, J. Heysch, B. Ladoux, J.P. Thiery, R.M. Mege, and S. Dufour. 2013. α-Catenin and vinculin cooperate to promote high E-cadherin-based adhesion strength. *J. Biol. Chem.* 288:4957–4969. https://doi.org/10.1074/jbc.M112.403774

Tilney, L.G., D.J. Derosier, and M.J. Mulroy. 1980. The organization of actin filaments in the stereocilia of cochlear hair cells. *J. Cell Biol.* 86:244–259. https://doi.org/10.1083/jcb.86.1.244

Truong Quang, B.A., M. Mani, O. Markova, T. Lecuit, and P.F. Lenne. 2013. Principles of E-cadherin supramolecular organization in vivo. *Curr. Biol.* 23:2197–2207. https://doi.org/10.1016/j.cub.2013.09.015

Twiss, F., and J. de Rooij. 2013. Cadherin mechanotransduction in tissue remodeling. *Cell. Mol. Life Sci.* 70:4101–4116. https://doi.org/10.1007/s00018-013-1329-x

Twiss, F., Q. Le Duc, S. Van Der Horst, H. Tabdili, G. Van Der Krogt, N. Wang, H. Rehmann, S. Huveneers, D.E. Leckband, and J. De Rooij. 2012. Vinculin-dependent Cadherin mechanosensing regulates efficient epithelial barrier formation. *Biol. Open.* 1:1128–1140. https://doi.org/10.1242/bio.20122428

Verkhovsky, A.B., T.M. Svitkina, and G.G. Borisy. 1995. Myosin II filament assemblies in the active lamella of fibroblasts: Their morphogenesis and role in the formation of actin filament bundles. *J. Cell Biol.* 131:989–1002. https://doi.org/10.1083/jcb.131.4.989

Verma, S., A.M. Shewan, J.A. Scott, F.M. Helwani, N.R. den Elzen, H. Miki, T. Takenawa, and A.S. Yap. 2004. Arp2/3 activity is necessary for efficient formation of E-cadherin adhesive contacts. *J. Biol. Chem.* 279:34062–34070. https://doi.org/10.1074/jbc.M404814200

Wu, Y., P. Kanchanawong, and R. Zaidel-Bar. 2015. Actin-delimited adhesion-independent clustering of E-cadherin forms the nanoscale building blocks of adherens junctions. *Dev. Cell.* 32:139–154. https://doi.org/10.1016/j.devcel.2014.12.003

Yamada, S., and W.J. Nelson. 2007. Localized zones of Rho and Rac activities drive initiation and expansion of epithelial cell–cell adhesion. *J. Cell Biol.* 178:517–527. https://doi.org/10.1083/jcb.200701058

Yamazaki, D., T. Oikawa, and T. Takenawa. 2007. Rac-WAVE-mediated actin reorganization is required for organization and maintenance of cell-cell adhesion. *J. Cell Sci.* 120:86–100. https://doi.org/10.1242/jcs.03311

Yao, M., W. Qiu, R. Liu, A.K. Efremov, P. Cong, R. Seddiki, M. Payre, C.T. Lim, B. Ladoux, R.M. Mège, and J. Yan. 2014. Force-dependent conformational switch of α-catenin controls vinculin binding. *Nat. Commun.* 5:4525. https://doi.org/10.1038/ncomms5525

Yap, A.S., G.A. Gomez, and R.G. Parton. 2015. Adherens junctions revisualized: Organizing cadherins as nanoassemblies. *Dev. Cell.* 35:12–20. https://doi.org/10.1016/j.devcel.2015.09.012

Yonemura, S. 2011. Cadherin-actin interactions at adherens junctions. *Curr. Opin. Cell Biol.* 23:515–522. https://doi.org/10.1016/j.ceb.2011.07.001

Yonemura, S., M. Itoh, A. Nagafuchi, and S. Tsukita. 1995. Cell-to-cell adherens junction formation and actin filament organization: similarities and differences between non-polarized fibroblasts and polarized epithelial cells. *J. Cell Sci.* 108:127–142.

Yonemura, S., Y. Wada, T. Watanabe, A. Nagafuchi, and M. Shibata. 2010. alpha-Catenin as a tension transducer that induces adherens junction development. *Nat. Cell Biol.* 12:533–542. https://doi.org/10.1038/ncb2055

Zhang, J., M. Betson, J. Erasmus, K. Zeikos, M. Bailly, L.P. Cramer, and V.M. Braga. 2005. Actin at cell-cell junctions is composed of two dynamic and functional populations. *J. Cell Sci.* 118:5549–5562. https://doi.org/10.1242/jcs.02639